iScience

CellPress
OPEN ACCESS

Article

Axin-Mediated Regulation of Lifespan and Muscle Health in *C. elegans* Requires AMPK-FOXO Signaling

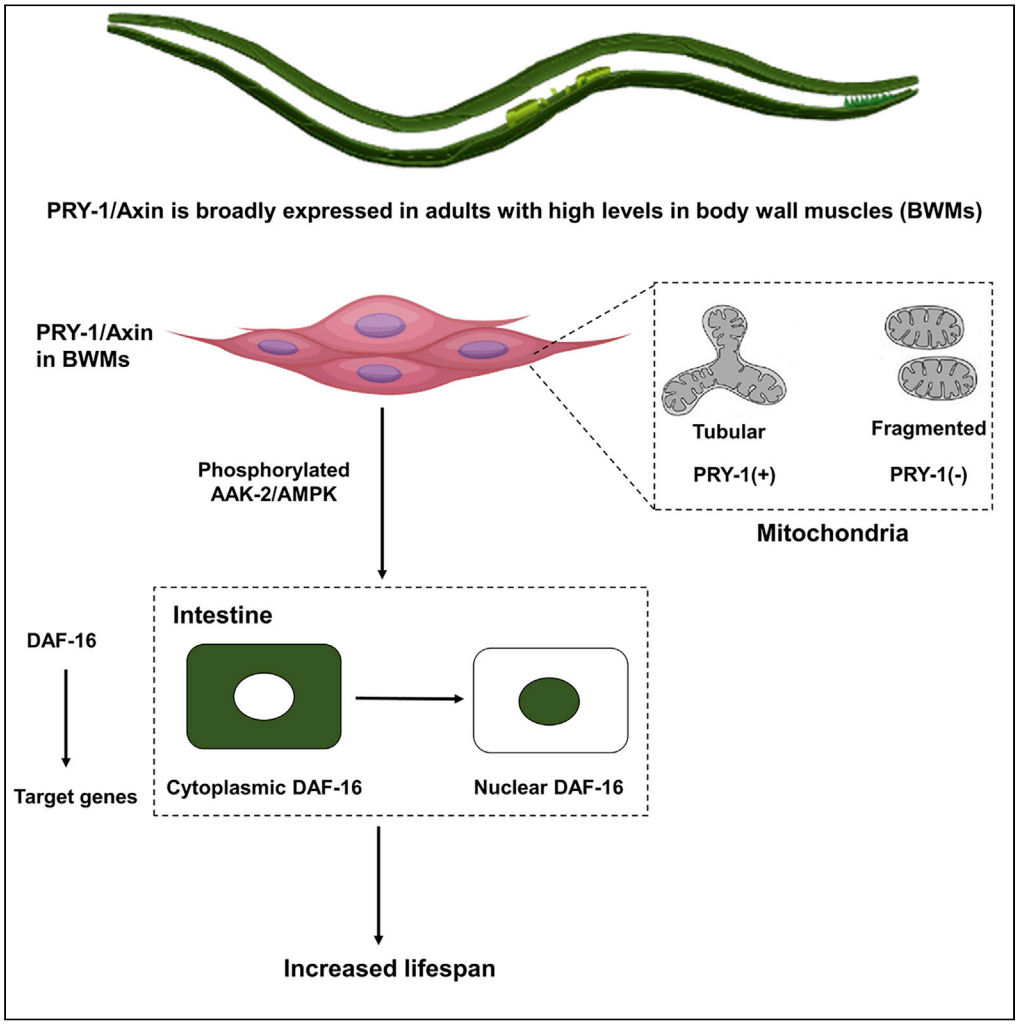

Avijit Mallick, Ayush Ranawade, Wouter van den Berg, Bhagwati P. Gupta

guptab@mcmaster.ca

HIGHLIGHTS

pry-1 transcriptome contains genes linked to aging and muscle function

pry-1 functions in muscles to maintain life span and mitochondrial network

Muscle-specific overexpression of *pry-1* extends life span and promotes muscle health

PRY-1-mediated life span extension depends on AAK-2-DAF-16 signaling

Mallick et al., iScience *23*, 101843
December 18, 2020
https://doi.org/10.1016/j.isci.2020.101843

iScience

CellPress
OPEN ACCESS

Article

Axin-Mediated Regulation of Lifespan and Muscle Health in *C. elegans* Requires AMPK-FOXO Signaling

Avijit Mallick,[1] Ayush Ranawade,[1,2] Wouter van den Berg,[1] and Bhagwati P. Gupta[1,3,*]

SUMMARY

Aging is a significant risk factor for several diseases. Studies have uncovered multiple signaling pathways that modulate aging, including insulin/insulin-like growth factor-1 signaling (IIS). In *Caenorhabditis elegans*, the key regulator of IIS is DAF-16/FOXO. One of the kinases that affects DAF-16 function is the AMPK catalytic subunit homolog AAK-2. In this study, we report that PRY-1/Axin plays an essential role in AAK-2 and DAF-16-mediated regulation of life span. The *pry-1* mutant transcriptome contains many genes associated with aging and muscle function. Consistent with this, *pry-1* is strongly expressed in muscles, and muscle-specific overexpression of *pry-1* extends life span, delays muscle aging, and improves mitochondrial morphology in AAK-2-DAF-16-dependent manner. Furthermore, PRY-1 is necessary for AAK-2 phosphorylation. Taken together, our data demonstrate that PRY-1 functions in muscles to promote the life span of animals. This study establishes Axin as a major regulator of muscle health and aging.

INTRODUCTION

Aging is defined as a progressive functional decline in living organisms. It is characterized by hallmarks such as genomic instability, epigenetic alterations, mitochondrial dysfunction, and telomere attrition, and is thought to be regulated in part by genetic pathways (Lopez-Otin et al., 2013). Several genes and pathways have been identified that govern and modulate life span and are conserved in higher eukaryotes (Kenyon, 2010; Lapierre and Hansen, 2012; Uno and Nishida, 2016). Insulin/insulin-like growth factor-1 signaling (IIS) was the first pathway shown to be involved in the regulation of aging in *Caenorhabditis elegans* (Kenyon, 2011; Kenyon et al., 1993). Subsequent studies have demonstrated that the IIS pathway is conserved across eukaryotes (Uno and Nishida, 2016). In *C. elegans*, reduction in the activity of the IIS receptor homolog DAF-2 leads to a prolonged life span, which is dependent on DAF-16, a FOXO transcription factor homolog (Kenyon et al., 1993). This modulation of life span by DAF-16 involves translocation to the nucleus followed by either the activation or repression of genes involved in stress response, metabolism, and autophagy (Lee et al., 2003; Melendez et al., 2003; Murphy et al., 2003).

The activity of DAF-16 is regulated by phosphorylation (Kenyon, 2010). One of the kinases involved in this process is the α2 catalytic subunit homolog of AMPK, AAK-2 (Greer et al., 2007a), a phenomenon that is conserved in the mammalian system (Greer et al., 2007b). AAK-2 also plays a crucial role in aging. It is essential for DAF-2-mediated life span extension, and its overexpression extends the life span of animals (Apfeld et al., 2004; Mair et al., 2011). Interestingly, a truncated version of AAK-2 bearing only the catalytic domain was found to be more effective than the full-length wild-type form, suggesting that AAK-2 activity is regulated during the normal aging process (Mair et al., 2011). As in *C. elegans*, AMPK in *Drosophila* is also involved in life span regulation. Specifically, overexpression of the α2 subunit in muscles and fat bodies extends the life span of transgenic animals (Stenesen et al., 2013).

AMPK is an established energy sensor in eukaryotes that is phosphorylated by several kinases, including LKB1 (Burkewitz et al., 2014; Hardie et al., 2012). Studies in mouse and human cell culture models have shown that, under the condition of glucose starvation, AMPK forms a complex with LKB1 and the scaffolding protein Axin (Zhang et al., 2013b). The multimeric complex regulates AMPK activation, leading to phosphorylation of downstream targets (Hardie and Lin, 2017; Hardie et al., 2012). The involvement of Axin in AMPK complex formation is essential, since Axin knockdown drastically reduces AMPK activity,

[1]Department of Biology, McMaster University, Hamilton, ON L8S-4K1, Canada

[2]Present address: Department of Bioengineering, Northeastern University, 360 Huntington Avenue, Boston, MA 02115

[3]Lead Contact

*Correspondence: guptab@mcmaster.ca

https://doi.org/10.1016/j.isci.2020.101843

leading to fatty liver in starved mice (Zhang et al., 2013b). In addition to their role in AMPK regulation, Axin family members are also involved in multiple biological processes during development and post-development (Mallick et al., 2019b). Since its discovery as a negative regulator of WNT signaling, Axin has been demonstrated to participate in other, non-WNT, pathways as well. In all cases, a common thread is Axin's role as a scaffold protein in recruiting other factors to form complexes (Mallick et al., 2019b). However, whether the scaffolding role of Axin affects FOXO activity remains to be investigated.

In this study, we report that the *C. elegans* Axin homolog PRY-1, which is necessary for embryonic and larval processes, is also essential for normal life span maintenance. Previously, it was found that metformin-mediated life span extension depends on another *C. elegans* Axin-like gene, *axl-1*. However, *axl-1* mutants do not show defects in aging and age-related processes (Chen et al., 2017). Our work has revealed that animals lacking *pry-1* function during adulthood are short-lived and show increased deterioration in aging-associated processes. Consistent with this, *pry-1* mutant transcriptome contains many aging-related protein-coding and miRNA genes. We found that *pry-1* is broadly expressed in adults, with high levels in body wall muscles (BWMs). Moreover, muscle-specific knockdown of *pry-1* caused an increase in the proportion of fragmented mitochondria and led to a reduction in life span. Conversely, overexpression of *pry-1* in muscles improved both phenotypes. Thus, *pry-1* appears to affect life span by regulating muscle mitochondria health. Interestingly, muscle-specific expression of mouse Axin (*mAxin1*) in *C. elegans* also extended life span, suggesting that Axin's role in aging may be conserved. It is worth mentioning that Axin is expressed in mouse and human skeletal muscles (Smith et al., 2019; Uhlen et al., 2015). To investigate PRY-1's mechanism of action, we performed a combination of molecular genetics and biochemical experiments. The results revealed that PRY-1's role in aging depends on AAK-2 and DAF-16. Our data suggest that PRY-1 presumably forms a complex with AAK-2 leading to its phosphorylation, thereby promoting nuclear localization of DAF-16 in the intestine and life span maintenance.

RESULTS

pry-1 Transcriptome Contains Genes Involved in Life Span Regulation

The involvement of PRY-1 in multiple signaling pathways and biological events is well documented (Mallick et al., 2019b). Earlier, we reported both mRNA and microRNA (miRNA) transcriptome profiles of *pry-1* mutant that revealed 2,665 differentially expressed protein-coding genes and six miRNAs (Mallick et al., 2019a; Ranawade et al., 2018). The characterization of differentially expressed genes showed *pry-1*'s crucial role in miRNA-mediated seam cell development (Mallick et al., 2019a) and lipid metabolism (Ranawade et al., 2018). In this study, we have specifically focused on the genes linked to aging. Of the differentially expressed miRNAs, *mir-246* is involved in aging and stress response (de Lencastre et al., 2010). The mRNA transcriptome dataset was analyzed using Gene Ontology (GO) terms, which revealed that aging-related protein-coding genes and gene families are overrepresented (69 in total; relative frequency (RF): 2, $p < 4.91 \times 10^{-9}$; 33% upregulated and 67% downregulated) and that they are linked to biological activities such as cellular processes (26 genes), metabolic processes (24 genes), and biological regulation (13 genes) (Figure 1A; Table S1). Within cellular processes, candidates include genes linked to lipid metabolism (*aap-1, hyl-1, elo-2, ctl-2, cat-1,* and *lipl-4*), which further supports the essential role of lipids in *pry-1*-mediated signaling (Ranawade et al., 2018) and suggests that *pry-1* may affect lipid metabolism to regulate aging.

Further GO term analysis of protein-coding aging-related genes showed that they are linked to 32 distinct signaling pathways and include well-known factors such as AAP-1 (PI3K adapter subunit) and DAF-16, both belonging to the IIS pathway (Lapierre and Hansen, 2012; Uno and Nishida, 2016), and XBP-1, a human XBP1 ortholog that acts downstream of IRE-1 and PEK-1-mediated signaling (Ron and Walter, 2007). Thus, *pry-1* appears to interact with multiple genetic networks. We also compared the *pry-1* transcriptome with differentially expressed genes of the DAF-2-DAF-16 signaling pathway (Lin et al., 2018) and found a significant overlap (415 genes; RF: 1.7, $p < 2.228 \times 10^{-31}$, Table S3). Additionally, 29 of 109 DAF-16 direct targets (Li and Zhang, 2016) are present in the *pry-1* dataset (27% overlap, $p < 0.01$; two-thirds downregulated), including four (*dod-17, prdx-3, nnt-1,* and *daf-16*) that are directly involved in aging (Figure 1B; Table S3). Taken together, these *in silico* analyses suggest that *pry-1* acts in part via DAF-16 to regulate life span in *C. elegans*.

Mutations in *pry-1* Reduce Life Span

In accordance with the above data suggesting *pry-1*'s role in aging, *pry-1* expression was found to be significantly higher in older adults (Figure S1A).We also found that the mean life span of *pry-1(mu38)* animals was 80% ($p < 0.001$) shorter compared with that of wild-type animals (Figure 1C; Table S2). A similar reduction in

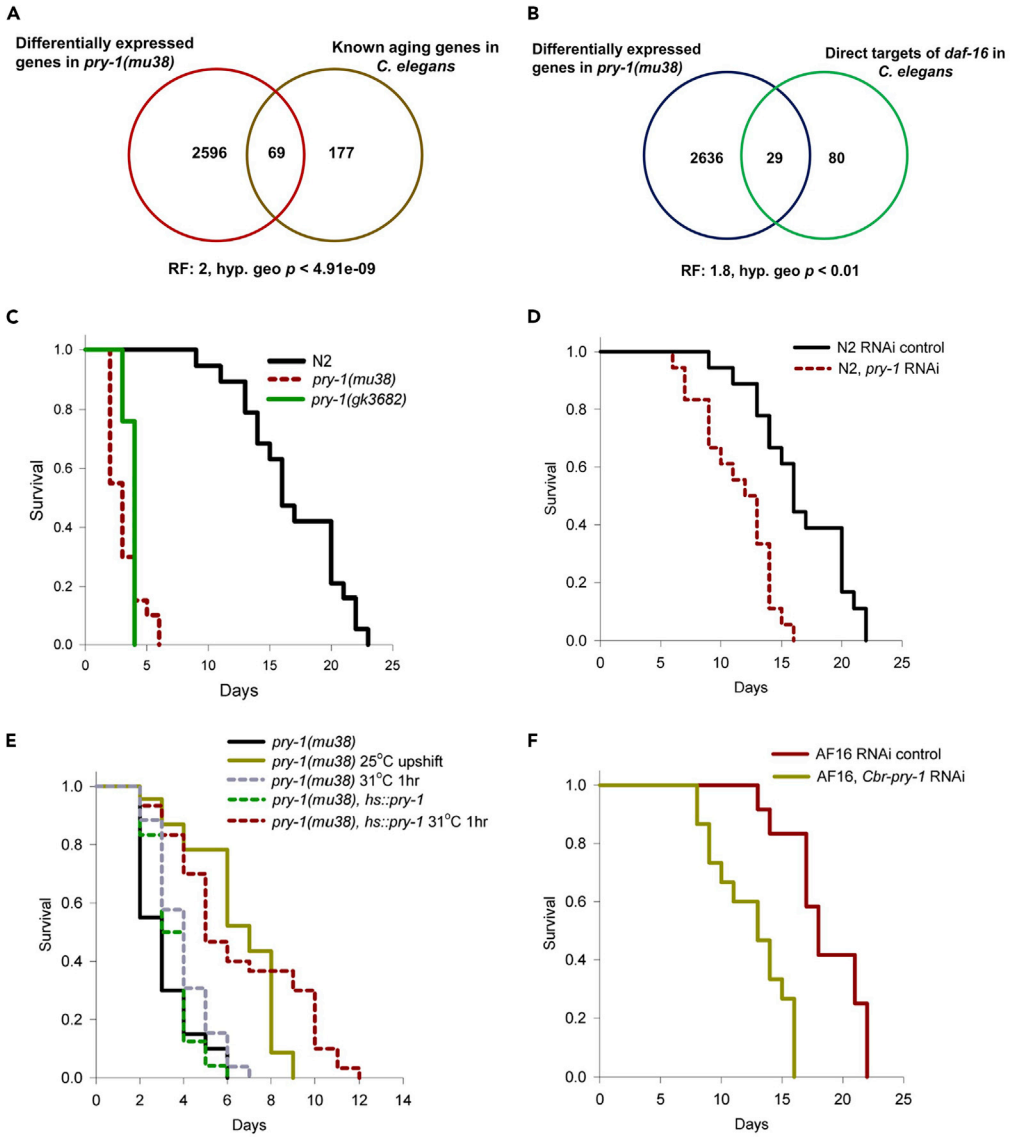

Figure 1. *pry-1* is Required for the Normal Life Span of Animals

(A) Sixty-nine differentially expressed genes in *pry-1* mutant transcriptome are linked to aging.

(B) More than a quarter of DAF-16 direct targets is present in *pry-1* mutant transcriptome.

(C) Life span of *pry-1(mu38)* animals.

(D) Life span of Adult-specific *pry-1(RNAi)* animals.

(E) Life span rescue experiments following two different treatments during adulthood, namely subjecting *pry-1(mu38)* to a 25°C upshift and 31°C 1hr heat-shock to *pry-1(mu38); hs::pry-1* animals. The control worms consist of *pry-1(mu38)* alone, *pry-1(mu38)* subjected to 31°C 1hr heat shock, and *pry-1(mu38); hs::pry-1* without heat shock.

(F) Life span analysis of *Cbr-pry-1(RNAi)* animals.

(E and F) See Transparent Methods and Table S2 for life span data and statistical analyses.

life span was also observed with a CRISPR allele, *gk3682,* that deletes a roughly 750-bp region, including the 5′ UTR and the first exon (Mallick et al., 2019a) (Figure 1C; Table S2). As *pry-1* is also involved in developmental processes (Mallick et al., 2019b), we took an RNAi approach to knock down the gene function specifically during adulthood. As expected, *pry-1(RNAi)* animals were found to be short-lived, with 22–31% ($p < 0.01$) reduced mean life span (Figure 1D; Table S2).

To further investigate whether *pry-1* affects aging, we performed two sets of rescue experiments. One of these involved making use of the cold-sensitive allele *mu38*. While the life span defect of *pry-1(mu38)* was

severe at 20°C (mean life span 81% lower than N2, $p < 0.001$, Figure 1E; Table S2), the animals appeared healthier and showed an improved life span at 25°C (50% lower than N2, $p < 0.01$, Figure 1E; Table S2). When day-1 *pry-1(mu38)* adults were upshifted from 20°C to 25°C, life span was extended by 107% (6.4 ± 0.4 days mean life span compared with 3.2 ± 0.1 days for untreated *mu38* control, $p < 0.01$). In the other experiment, transgenic animals were generated carrying a heat-shock promoter-driven *pry-1*. The *hs::pry-1* transgene efficiently rescued the life span defect of *pry-1(mu38)* animals upon heat-shock during adulthood (58% longer mean life span compared to control animals, $p < 0.001$, Figure 1E; Table S2). Interestingly, no such effect was observed when the transgene was expressed in wild-type background (Figure S1B; Table S2).

Since our lab had previously reported a conserved role of *C. briggsae pry-1* during development (Seetharaman et al., 2010), we investigated whether *Cbr-pry-1* is also involved in aging. The results revealed both the *sy5353* mutant allele and adult RNAi caused a shorter life span in animals (Figures 1F and S1C; Table S2). These data show that *pry-1* function in life span maintenance is conserved in nematodes.

pry-1 Knockdown in Adults Causes Accelerated Aging and Increased Expression of Stress Response Markers

Several physiological and molecular changes occur in animals during the aging process. These include a decline in tissue function, oxidative stress, accumulation of mis/unfolded proteins, and altered lipid distributions (Huang et al., 2004; Lopez-Otin et al., 2013). To characterize such changes in *pry-1(RNAi)* animals, we analyzed the age-dependent decline in pharyngeal pumping and body bending. Adult-specific knockdown led to a significant reduction in rates of pharyngeal pumping and body bending starting on days 7 and 2, respectively (Figures 2A and 2B). Similar phenotypes were also observed in *pry-1(mu38)* mutants, although the defects were more severe (Figures S2A and S2B). Consistent with the adult-specific role of *pry-1*, we found that heat-shocked *pry-1(mu38); hs::pry-1* adults showed significant improvements in both these aging-related markers (Figures S2C and S2D). Together, the results demonstrate that *pry-1* is needed to delay aging-associated physical deterioration in animals.

Next, we measured lipofuscin levels in adults. In *C. elegans*, lipofuscin, a product of oxidative damage and autophagy, is visible as auto fluorescent granules in the intestine and serves as a biomarker of aging (Davis et al., 1982). Quantification of the intestinal autofluorescence showed a 30% increase ($p < 0.05$) in *pry-1(RNAi)* adults compared with that in N2 control animals (Figures 2C and 2D). The expression of an oxidative stress marker, manganese superoxide dismutase (*sod-3*), was also investigated (Lopez-Otin et al., 2013). The RNAi-mediated knockdown of *pry-1* caused no significant change in *sod-3:GFP* fluorescence (Figures 2C and 2D), suggesting that *pry-1* function is not essential for the maintenance of oxidative stress.

Other indicators of premature aging include unfolded protein response (UPR) associated with mitochondria and ER (UPR^{MT} and UPR^{ER}, respectively) (Lopez-Otin et al., 2013). Upon activation, these UPR pathways increase the expression of chaperones and heat shock proteins such as *hsp-6* and *hsp-60* (UPR^{MT}) (Tran and Van Aken, 2020) and *hsp-4/Bip* (UPR^{ER}) (Ron and Walter, 2007). We found that GFP fluorescence of all three markers, namely *hsp-6::GFP*, *hsp-60::GFP*, and *hsp-4::GFP*, was significantly increased in *pry-1(RNAi)* day-8 adults compared with that in controls (70%, 40%, and 50% higher, respectively, $p < 0.01$) (Figures 2C and 2D). Moreover, it was observed that *pry-1* transcriptome contains genes involved in IRE-1/IRE1 and PEK-1/PERK-mediated UPR^{ER} signaling (57 genes, 49% overlap, R.F. 3.2, $p < 5.87 \times 10^{-18}$; and 10 genes, 43% overlap, R.F. 2.9, $p < 0.001$, respectively) (Table S4), including the key downstream factor, XBP-1, which activates *hsp-4* expression (Ron and Walter, 2007).

Collectively, the above data provide evidence that *pry-1* plays an essential role in the maintenance of aging-associated processes and stress response in animals. One possibility may be that *pry-1* affects aging by regulating lipid metabolism. This is supported by our previous results demonstrating that lipid synthesis is compromised in *pry-1* mutant animals (Mallick and Gupta, 2020; Ranawade et al., 2018). More importantly, adult-specific knockdown of *pry-1* caused a significant reduction in lipid content in day-8 adults (Figure 2E). Given that *daf-16* is also necessary for lipid synthesis (Murphy et al., 2003; Ogg et al., 1997; Zhang et al., 2013a) and *pry-1* and *daf-16* transcriptomes contain a common set of lipid synthesis and transport genes (such as *fat-5-7* and *vit-1/3/4/5*) (Table S3), it is conceivable that *pry-1* and *daf-16* interact to regulate lipid levels, leading to a normal life span of animals.

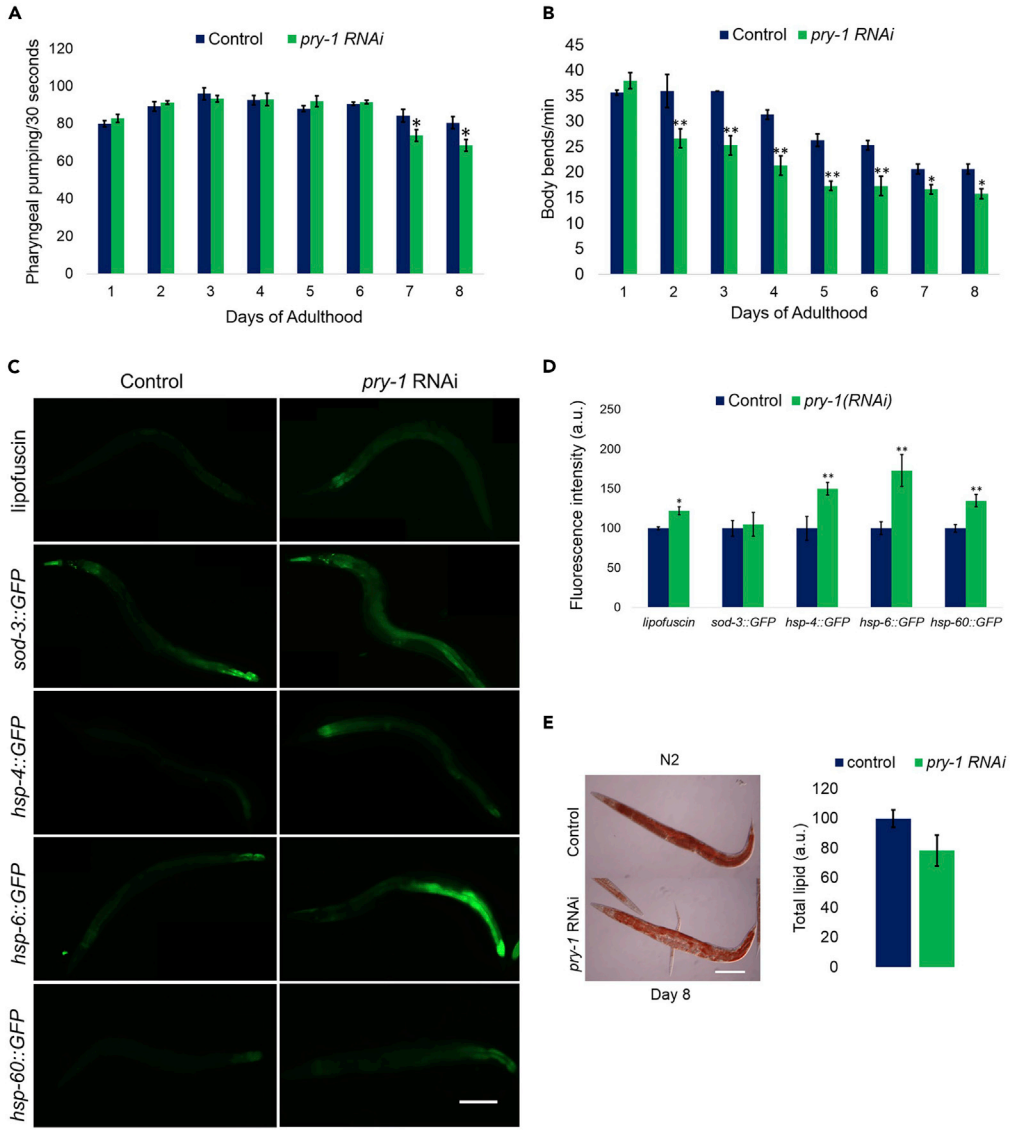

Figure 2. Adult-Specific Lowering of *pry-1* Accelerates Aging-Associated Markers

(A and B) Pharyngeal pumping of RNAi-treated *pry-1* in day-7 and day-8 adults (A) and body bending starting day-2 of adulthood (B). Data represent the mean of at least two replicates (n ≥ 30 animals) and error bars represent the standard deviation. Significance was calculated using Student's t-test *p < 0.05, **p < 0.01.

(C) Representative images of animals showing aging pigment (lipofuscin), ROS marker (*sod-3::GFP*), UPR-ER marker (*hsp-4::GFP*), and UPR-MT markers (*hsp-6::GFP* and *hsp-60::GFP*). Scale bar is 0.1mm.

(D) Quantification of fluorescence intensity shown in panel C.

(E) Oil red O staining of total lipid droplets in day-8 control and *pry-1(RNAi)* animals. Scale bar is 0.1mm. (D and E) Data represent the mean of two replicates (n ≥ 15 animals in each), and error bars represent the standard deviation. Significance was calculated using Student's t-test. **p < 0.01.

pry-1 Knockdown Suppresses Life Span Extension of *mom-2/WNT* Mutants

As PRY-1 is an established negative regulator of WNT signaling, we examined its genetic interactions with WNT ligands. Of the five known ligands, loss-of-function mutations in *mom-2* and *cwn-2* cause an extension of life span (Lezzerini and Budovskaya, 2014). When *pry-1* was knocked down in *mom-2(or42)* and *cwn-2(ok895)* backgrounds, life span extension was significantly reduced in *mom-2* mutants (13.6% reduction in mean life span, $p < 0.05$, Figure 3A; Table S2) but remained unchanged in the *cwn-2* animals (Figure 3B; Table S2). We also analyzed the requirements of *bar-1/β-catenin*, a component of the canonical WNT signaling that plays a role in aging (Xu et al., 2019; Zhang et al., 2018), in the *mom-2-pry-1* pathway. Since

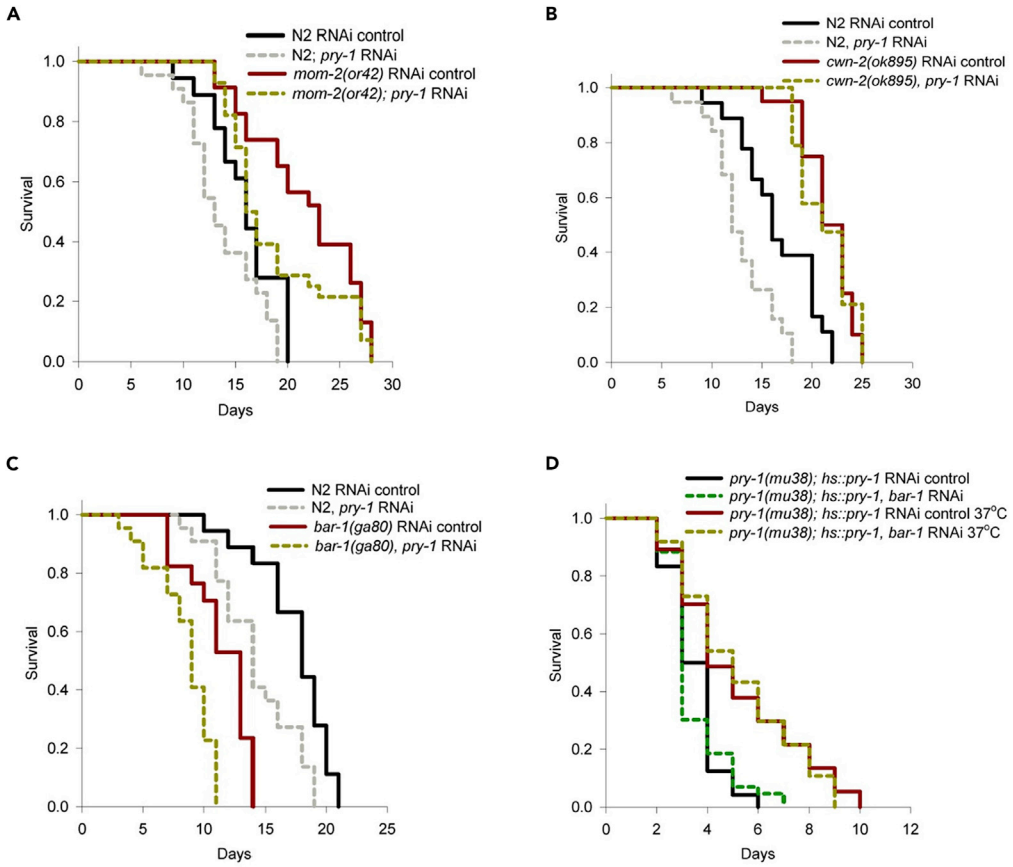

Figure 3. *pry-1* Functions Downstream of WNT Ligand *mom-2* and Independently of β-Catenin *bar-1* to Regulate Life Span

(A–C) Life span analysis following RNAi knockdown of *pry-1* in WNT pathway mutants, *mom-2(or42)* (A), *cwn-2(ok895)* (B), and *bar-1(ga80)* (C).

(D) Effect of *bar-1* RNAi in *pry-1(mu38); hs::pry-1* animals.

(A–D) See Transparent Methods and Table S2 for life span data and statistical analyses.

pry-1-mediated WNT signaling negatively regulates *bar-1*, removing *bar-1* function is expected to suppress the phenotype of *pry-1* mutants. However, we observed that the life span of *bar-1* null mutants was further shortened by *pry-1* RNAi (Figure 3C; Table S2), suggesting that *bar-1* is unlikely to participate in the *pry-1*-mediated aging process. Further support for this model comes from a *bar-1* RNAi experiment that failed to suppress the life span phenotype of *pry-1(mu38); hs::pry-1* animals (Figure 3D; Table S2). These data suggest that PRY-1 may act downstream of MOM-2 in a pathway that is independent of BAR-1 and likely to utilize DAF-16-mediated signaling.

Tissue-Specific Analysis Shows that *pry-1* is Needed in Muscles and Hypodermis

To investigate the requirements of *pry-1* in life span regulation, we examined its *in vivo* expression pattern. Previously, a 3.6-kb *pry-1* proximal promoter was used to drive the coding sequence of *pry-1* fused to a *GFP* reporter, which showed fluorescence throughout development, specifically in the vulval precursor cells, neurons, BWM, and some hypodermal cells (Korswagen et al., 2002). We further characterized *pry-1* expression, which revealed expression in almost all tissues during development. Expression in seam cells, neuronal cells, muscles, hypodermis, and intestine was readily visible (Figure 4A). This pattern of localization matches well with tissue enrichment of differentially expressed genes in the *pry-1* transcriptome using WormBase tissue ontology tool (Table S5, see Transparent Methods). The most enriched tissues include neurons and muscles.

A closer examination of GFP localization in developing animals revealed bright fluorescence in the ventral cord region, which includes neuronal and non-neuronal cells. The expression was largely similar in adults, although

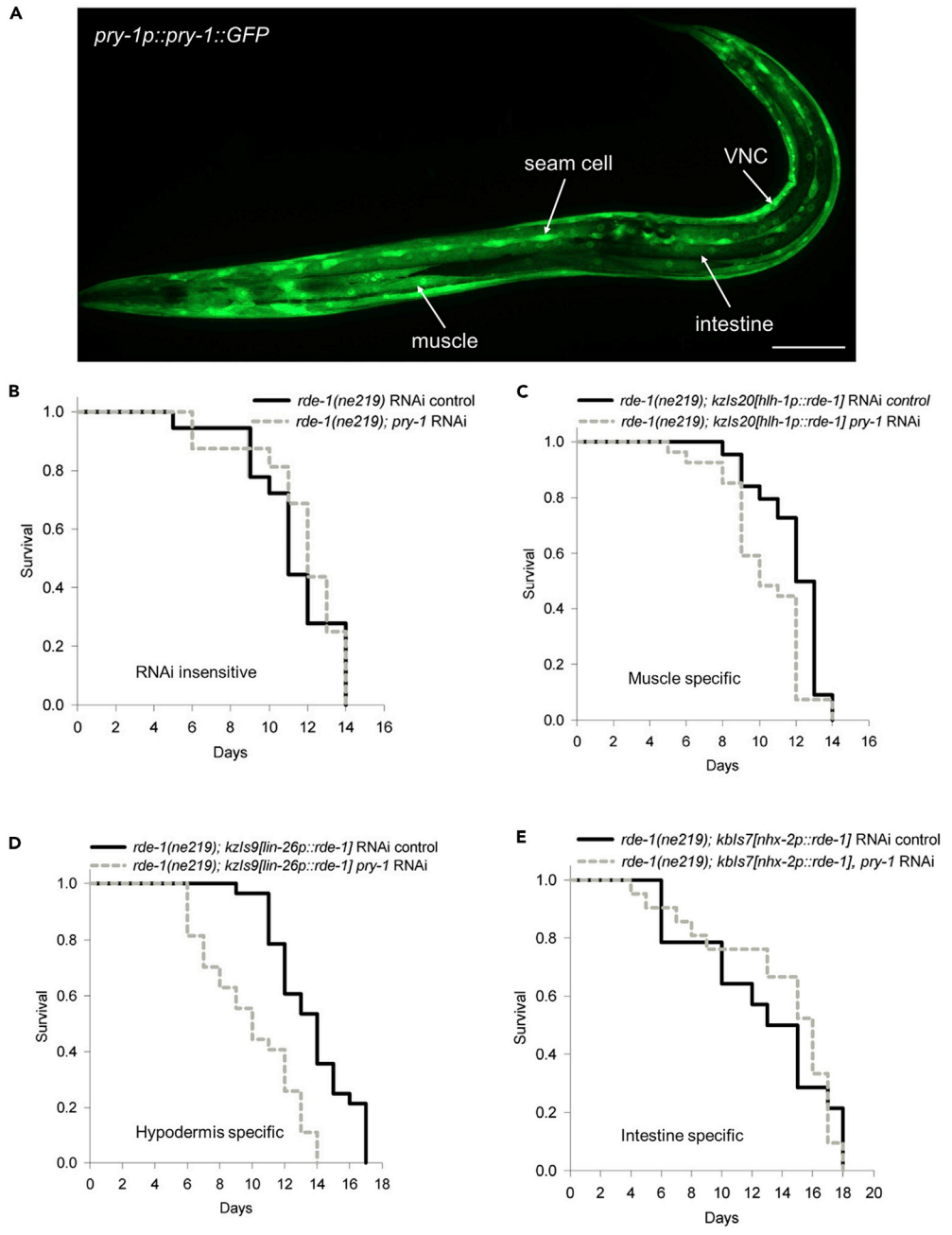

Figure 4. Expression Pattern of *pry-1* in Adults and Its Tissue-Specific Requirements for Life Span Maintenance

(A) Representative image of *pry-1p::pry-1::GFP* animals showing GFP fluorescence in muscles, intestine, seam cells, and neurons. Also see Figure S3. Scale bar is 0.1mm.

(B–E) Life span analysis after tissue-specific RNAi knockdown of *pry-1*. Also see Figures S4B and S4C *pry-1* RNAi knockdown control (B) and *pry-1* RNAi knockdown in muscle (C), hypodermis (D), and intestine (E). (B–E) See Transparent Methods and Table S2 for life span data and statistical analyses.

the fluorescence was much higher in BWMs (Figures 4A, S3A, and S3B). The posterior end of the intestine, near the rectal opening, showed a strong signal in L4 and adult animals; however, the rest of the intestine lacked a detectable expression. In general, GFP was diffused and not localized to any specific subcellular structures except in the case of muscles and posterior intestine, where nuclei are visible (see arrows in Figures S3B and S3C). The fluorescence continued to persist in older adults, consistent with the role of *pry-1* in aging. A similar pattern of expression for *pry-1* was also observed in *C. briggsae* transgenic animals, with a marked increase in

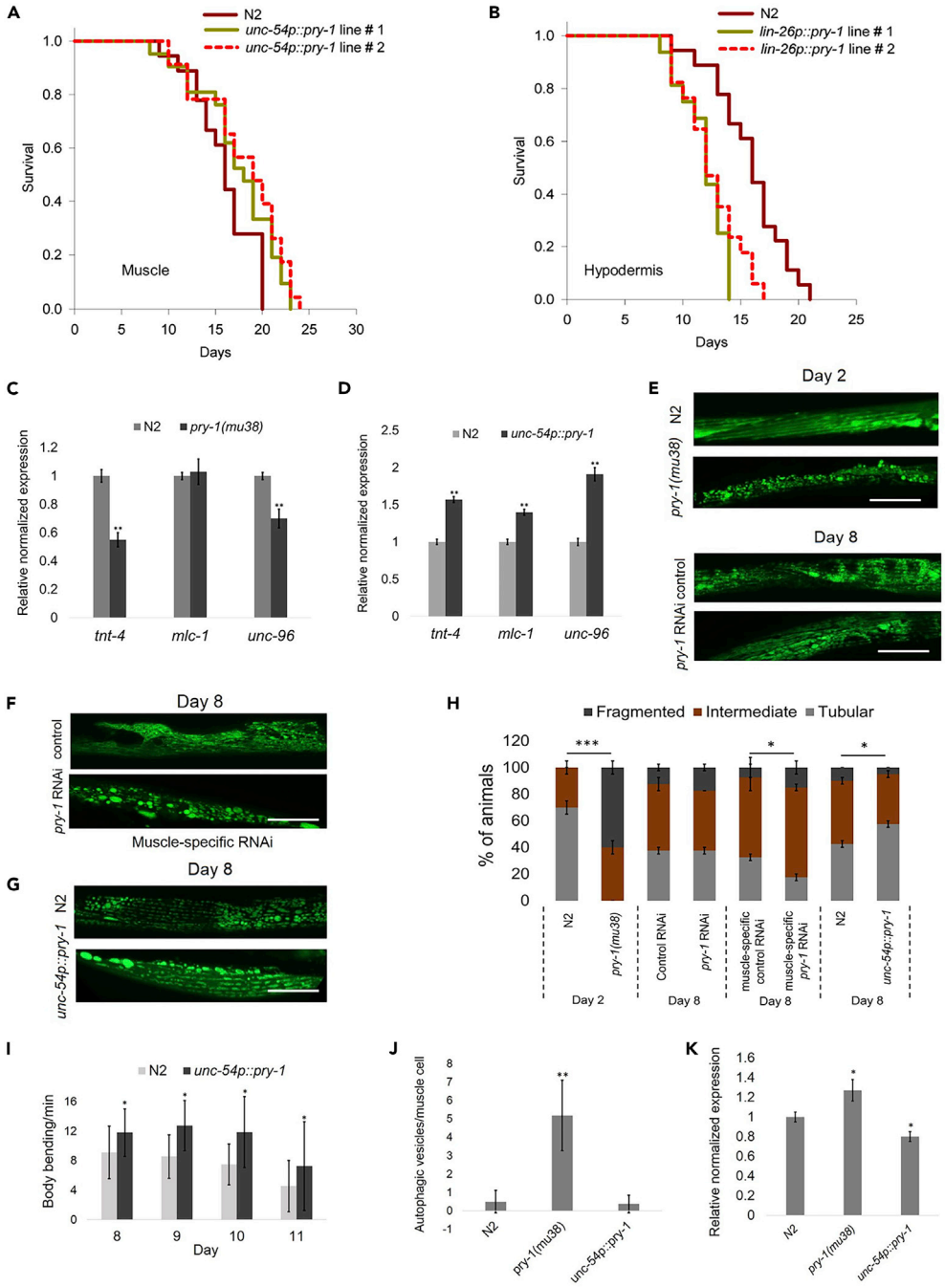

Figure 5. *pry-1* Overexpression in the Muscle Extends Life Span and Improves Muscle Physiology

(A and B) Effects of tissue-specific overexpression of *pry-1*. Overexpression in muscle (A), also see Figure S5B and Table S2, and in hypodermis (B). See Transparent Methods and Table S2 for life span data and statistical analyses.

(C and D) qPCR analysis of muscle genes *tnt-4*, *mlc-1* and *unc-96* in day-1 *pry-1(mu38)* (C) and *unc-54p::pry-1* (D) adults. Data represent the mean of two replicates and error bars represent the SEM. Significance was calculated using Bio-Rad software (t test). **p < 0.01.

(E–G) Representative images of muscle mitochondrial morphologies revealed by *myo-3p::GFP(mito)* reporter in the control, *pry-1(mu38)*, *pry-1(RNAi)*, and *unc-54p::pry-1* transgenic animals. The control for whole-animal RNAi experiment was N2 (E) and for muscle-specific RNAi was an RNAi-sensitive strain (F), each fed with bacteria carrying an empty vector (L4440) (see Transparent Methods for genotypes). Day-2 adults were used for *pry-1(mu38)*, whereas day-8 adults for *pry-1(RNAi)* and *unc-54p::pry-1* animals. Scale bar is 25μm.

Figure 5. *Continued*

(H) Quantification of phenotypes in panels E, F, and G. Data represent the mean of two replicates (n = 20 animals in each) and error bars standard deviations. Statistical analyses were carried out using the two-tailed Fisher's exact test by comparing mitochondrial morphology between normal (tubular) and defective (intermediate and fragmented) categories and indicated by stars (*). *p < 0.05, ***p < 0.0001. See Transparent Methods for details.

(I) Body bending analysis of *unc-54p::pry-1* adults between day-8 and day-11. Also see Figure S5D.

(J) Number of autophagic vesicles per muscle cell at day-2 of adulthood revealed by *dyc-1S::lgg-1::GFP*, a GFP marker of autophagic vesicles in body-wall muscles. (I-J) Data represent the mean of two replicates (n ≥ 15 animals in each) and error bars standard deviations. Significance was calculated using Student's t-test. *p < 0.05, **p < 0.01.

(K) *lgg-1* transcript levels in *pry-1(mu38)* and *unc-54p::pry-1* animals. Data represent the means of two replicates and error bars the SEM. Significance was calculated using Bio-Rad software (t test). *p < 0.05.

fluorescence in muscles throughout adulthood (Figure S4A). This pattern of *pry-1* expression in both nematodes suggests that the gene may play a conserved role in maintaining muscle health during aging.

Given that *pry-1* is expressed in muscles as well as other tissues, we examined its tissue-specific requirements for life span maintenance. To this end, RNAi experiments were performed in adults using strains that allow tissue-specific knockdowns in muscles, hypodermis, intestine, and neurons (see Transparent Methods). The results showed that *pry-1* RNAi caused a significant reduction in mean life span when knocked down in the hypodermis and muscles (26% lower mean life span in hypodermis RNAi and 12% in muscle RNAi, $p < 0.05$) (Figures 4B–4D). No such effect was observed in other tissues (Figures 4E, S4B, and S4C). We conclude that *pry-1* functions in muscles and hypodermis to maintain the life span of animals. Further support for this comes from the analysis of transgenic strains in which *pry-1* expression was driven by hypodermal and muscle-specific promoters (*lin-26p::pry-1* and *unc-54p::pry-1,* respectively). In both cases, the life span defect of *pry-1(mu38)* animals was significantly rescued (41% and 56% increases in mean life span by *lin-26p::pry-1* and *unc-54p::pry-1,* respectively, $p < 0.01$) (Figures S5A and S5B; Table S2).

Having uncovered the role of *pry-1* in hypodermis and muscles, we examined whether overexpression of the gene in these two tissues can extend the life span. Interestingly, while muscle-specific expression (*unc-54p::pry-1*) extended the life span significantly (13% increase in mean life span, $p < 0.05$), no such effect was observed in the case of hypodermis-specific expression (*lin-26p::pry-1*) (Figures 5A and 5B; Table S2). In fact, *lin-26p::pry-1* animals were short-lived, suggesting that a lack of spatiotemporal control is detrimental (Figure 5B; Table S2). These data, together with RNAi and rescue experiments, firmly establish that *pry-1* functions in both muscles and hypodermis for the maintenance of life span, and its hypodermal expression needs to be tightly regulated. Furthermore, the results have revealed a role of *pry-1* in muscles that is beneficial to animals throughout the life span. Interestingly, muscle-specific expression of *mAxin1* also caused animals to live longer (14% increase in mean life span, $p < 0.05$) (Figure S5C; Table S2).

Overexpression of *pry-1* in Muscles Improves Muscle Health and Mitochondrial Morphology

The life span extension observed in *unc-54p::pry-1* animals led us to investigate the cellular and molecular basis of *pry-1*'s role in muscle health. Based on GO analysis, we found that *pry-1* transcriptome contains a significant number of muscle-associated genes (31 of 123, 25.2%, R.F. 1.7, $p < 0.002$) (Table S5). A majority of these genes are downregulated (90.3%, 28 of 31 genes), suggesting that *pry-1* is needed to maintain their expression. Further investigation identified two broad categories, namely muscle structure development (21 genes) and muscle contraction (15 genes) (Table S5), both of which include core components of the sarcomere, such as the subunits of troponin complex (*tnt-3, tnt-4*), twitchin/titin (*unc-22*), myosin complex (*mlc-1, unc-15, unc-54*), and voltage-gated potassium channels (*unc-58, unc-103, slo-1*) (Table S5). We chose three genes at random to validate changes in their expression by quantitative Polymerase Chain Reaction (qPCR): *mlc-1* and *tnt-4* (involved in muscle contraction and structure development), and *unc-96* (involved in muscle structure development). The results confirmed that *tnt-4* and *unc-96* were indeed downregulated in *pry-1(mu38)* mutants, whereas *mlc-1* expression was unchanged (Figure 5C). As expected, all three genes were upregulated in *unc-54p::pry-1* animals (Figure 5D).

Since muscle health is linked to mitochondrial homeostasis (Gouspillou and Hepple, 2016; Hood et al., 2019; Mergoud Dit Lamarche et al., 2018; Regmi et al., 2014), we speculated that *pry-1* is necessary to maintain the expression of mitochondrial genes. Indeed, genes associated with mitochondrial structure and function are overrepresented in the *pry-1* transcriptome (173 genes, 27%, R.F. 1.8, $p < 1.691 \times 10^{-15}$) (Table S6). These include genes that function in the mitochondrial membrane (52 of 220, 24% overlap, R.F. 1.6, p <

5.567 × 10^{-4}), mitochondrial outer membrane (10 of 30, 33% overlap, R.F. 2.2, $p < 0.01$), mitochondrial matrix (37 of 137, 27% overlap, R.F. 1.8, $p < 2.298 \times 10^{-4}$), and mitochondrial gene expression (18 of 53, 34% overlap, R.F. 2.2, $p < 5.146 \times 10^{-4}$) (See also Table S6).

Further support of *pry-1*'s role in mitochondrial health comes from examination of BWMs using an organelle-specific GFP reporter, mitoGFP (Benedetti et al., 2006). The mitoGFP was used earlier to demonstrate age-dependent fragmentation of muscle mitochondria and, consequently, the loss of muscle function, since significantly fewer adults exhibited a tubular mitochondrial morphology (Mergoud Dit Lamarche et al., 2018; Regmi et al., 2014). We found that while muscle-specific, but not whole animal, *pry-1* RNAi caused a subtle but statistically significant defect in mitochondria in older adults, *pry-1(mu38)* animals exhibited a drastic increase in fragmented mitochondria (Figures 5E, 5F, and 5H). In contrast, the morphology was better preserved in *unc-54p::pry-1* adults compared with wild-type controls (Figures 5G and 5H), demonstrating that *pry-1* is needed to maintain muscle mitochondrial homeostasis.

The above results led us to investigate whether the mitochondrial network architecture mirrors the functional state of muscles. Studies have shown that the loss of locomotion and pharyngeal pumping are associated with fragmented mitochondrial structure in older worms (Mergoud Dit Lamarche et al., 2018; Regmi et al., 2014). Since a similar correlation is also seen in *pry-1(mu38)* day-1 adults, we wondered whether *unc-54p::pry-1* animals will appear healthier with respect to these aging-related markers. The experiments revealed that, while overexpression of *pry-1* in muscles led to a significantly improved body bending rate in adults, pharyngeal pumping and thrashing were comparable to that of controls (Figures 5I and S5D–S5F). These results are consistent with *pry-1*'s role in maintaining the mitochondrial network, which may contribute to the improvement of muscle health.

Another process that affects muscle aging is autophagy, in which damaged mitochondria are selectively removed (Madeo et al., 2015; Twig and Shirihai, 2011). While autophagy is beneficial for longevity, its effect is detrimental in the presence of increased mitochondrial permeability, which triggers mitochondrial fragmentation (Zhou et al., 2019). Since muscle autophagy increases with age (Mergoud Dit Lamarche et al., 2018), we investigated whether the process is affected in *pry-1* mutants that are short-lived. The analysis of autophagic vesicles, using *dyc-1S::lgg-1::GFP* marker (Mergoud Dit Lamarche et al., 2018), revealed that vesicle number per muscle cell was significantly higher in *pry-1(mu38)* animals compared with that in controls (Figure 5J). Similar results were also obtained by the analysis of *lgg-1* transcripts (Figure 5K). As expected, no such effect was found in the *unc-54p::pry-1* genetic background (Figures 5J and 5K). Overall, our data demonstrate that *pry-1* regulates muscle mitochondrial morphology to maintain muscle structure and function.

daf-16/FOXO Functions Downstream of *pry-1* to Maintain Life Span

As described above, we found that *daf-16* is downregulated in the *pry-1* transcriptome. *daf-16* encodes several isoforms, three of which, R13H8.1b, d, and f (WormBase WS261 release), influence the rate of the aging process (Chen et al., 2015; Kwon et al., 2010). To examine whether *pry-1* affects these isoforms, we performed qPCR analysis. In the case of *pry-1(mu38)*, transcripts for R13H8.1b/c (*daf-16a*) and R13H8.1d/f/h/i/k (*daf-16d/f/h/i/k*) were significantly downregulated (Figure S6A). An opposite trend was observed in *unc-54p::pry-1* animals (Figure S6B). How might *pry-1* regulate transcription of *daf-16*? Previously, two intestinal GATA transcription factors, *elt-2* and *elt-4*, were shown to promote *daf-16* transcription, leading to longevity (Bansal et al., 2014). Using qPCR, we found that the expression of both *elt-2* and *elt-4* was significantly upregulated in the muscle-specific line (*unc-54p::pry-1*) (Figure S6C). Thus, *pry-1* may use these GATA factors directly or indirectly to affect *daf-16* transcription.

To investigate whether the interaction of *pry-1* with *daf-16* is affected by *daf-2* signaling (IIS), we knocked down *pry-1* in both *daf-2* and *daf-16* mutant backgrounds. While the knockdown caused a reduction in *daf-2(e1370ts)* life span (Figure S6D), no change was observed in *daf-16(mu86)* animals (Figure 6A), suggesting that *pry-1* may act genetically downstream of *daf-2* but upstream of *daf-16*. The results of the following two experiments are most consistent with the possibility of *daf-16* acting downstream of *pry-1*: One, *daf-16* RNAi suppressed the life span extension observed in *pry-1(mu38); hsp::pry-1* animals (Figure S6E), and, two, life span defect of *pry-1(mu38)* animals is significantly rescued by *daf-16* overexpression (Figure 6B).

Since DAF-16's function depends on its nuclear localization (Kenyon, 2010), we investigated whether PRY-1 plays a role in this process. The fluorescence of DAF-16:GFP in *unc-54p::pry-1* animals was localized

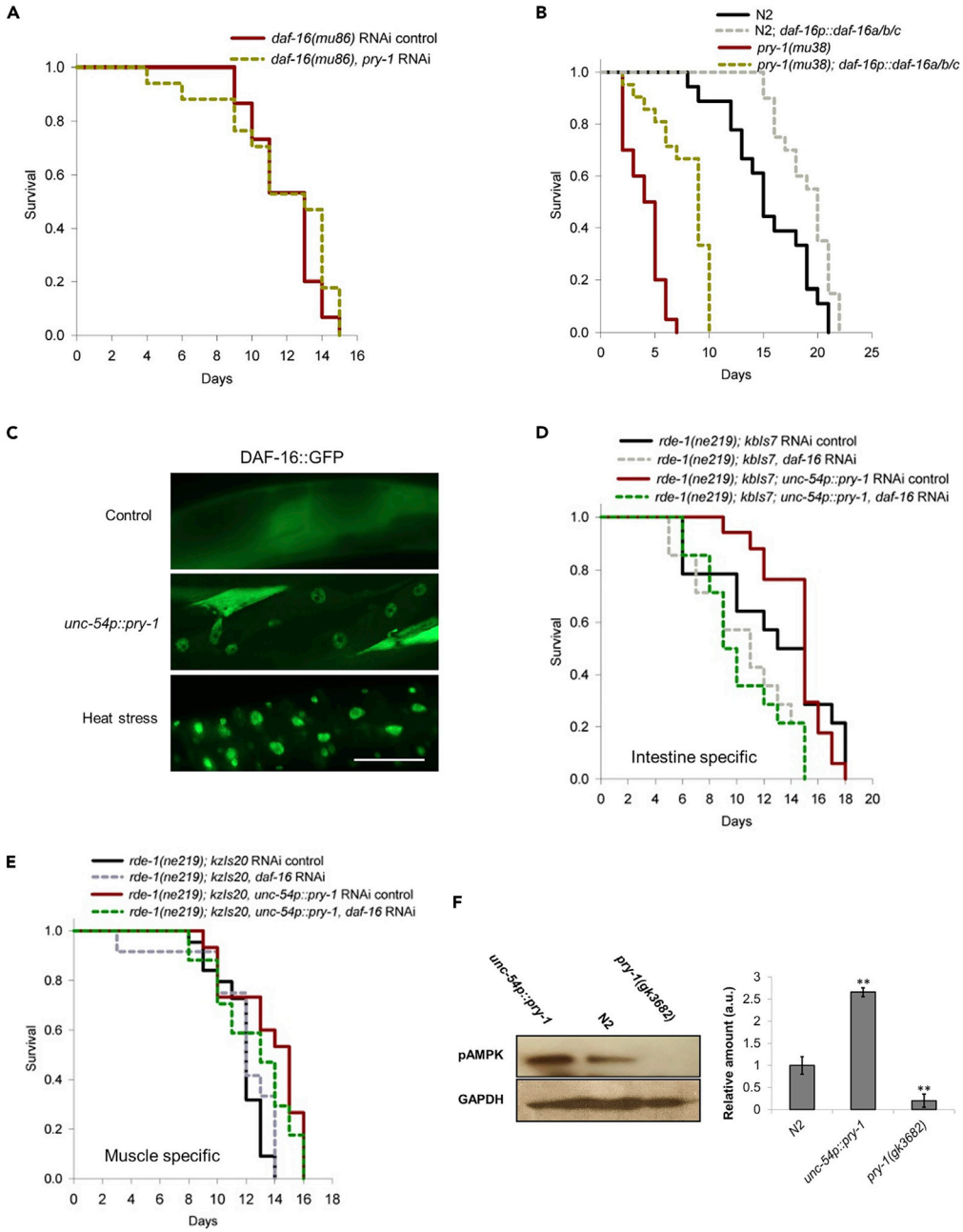

Figure 6. Life Span Regulation by *pry-1* Depends on *daf-16* Function in the Intestine

(A) *pry-1* RNAi knockdown in *daf-16(mu86)* animals.

(B) *daf-16* overexpression in *pry-1(mu38)* animals.

(C) Localization of GFP fluorescence in *unc-54p::pry-1* intestinal nuclei. Scale bar is 50μm. 100% of the *unc-54p::pry-1* animals (n = 30) showed nuclear localization for DAF-16:GFP.

(D and E) Intestine-specific *daf-16* RNAi knockdown (D) and muscle-specific knockdown (E) in *unc-54p::pry-1* animals.

(A, B, D, and E) See Transparent Methods and Table S2 for life span data and statistical analyses.

(F) Western blot analysis of AAK-2 phosphorylation in control, *pry-1* mutant, and *unc-54p::pry-1* animals. Data represent the means of two replicates and error bars the standard deviation. Significance was calculated using Student's t-test. **$p < 0.01$.

frequently to intestinal nuclei (Figure 6C). Consistent with this, *sod-3,* a direct target of *daf-16*, was overexpressed (Figure S6F). The transgenic worms also exhibited a higher level of lipids (Figures S7A and S7B), which supports *pry-1's* role in lipid synthesis (Mallick and Gupta, 2020; Ranawade et al., 2018). Moreover, there was a significant up-regulation of fatty acid desaturases (*fat-5, fat-6,* and *fat-7*) and the SREBP homolog *sbp-1* (Figure S7C). These findings, along with the known role of *daf-16* in promoting lipid synthesis (Papsdorf and Brunet, 2019), lead us to propose that *pry-1* interacts with *daf-16* to regulate lipids.

To examine whether *daf-16* acts locally in the intestine or via a long-range signal by functioning in the muscle, we performed tissue-specific RNAi experiments. Life span extension of *unc-54p::pry-1* was completely abolished by *daf-16* knockdown in the intestine (Figure 6D), the tissue where it acts primarily to regulate life span (Libina et al., 2003). No such effect was observed following muscle-specific knockdown (Figure 6E). Overall, the results show that *daf-16* is involved in *pry-1*-mediated life span regulation and that life span extension observed in muscle-overexpressed *pry-1* animals depends on *daf-16* function in the intestine.

DAF-16-Mediated PRY-1 Signaling Depends on AAK-2 Function

Next, we determined the nature of interaction between *pry-1* and *daf-16*. In the mammalian system, Axin forms a complex with AMPK and LKB1 upon glucose starvation, resulting in phosphorylation of AMPK (Zhang et al., 2013b). The activated AMPK, in turn, phosphorylates a number of targets, including FOXO family members, preferentially FOXO3 (Greer et al., 2007b; Mihaylova and Shaw, 2011). Since the AMPK-FOXO interaction also occurs in *C. elegans* where AAK-2 phosphorylates DAF-16 and plays a role in DAF-16-dependent life span extension (Greer et al., 2007a; Mair et al., 2011), we investigated whether PRY-1 is involved in activating AAK-2. For this, AAK-2 phosphorylation was quantified in worm protein extracts. The results showed that, while the phosphorylated AAK-2 level was drastically reduced in *pry-1* mutants when probed with phospho-AMPK (T172) antibody, it was significantly increased in *unc-54p::pry-1* animals (Figure 6F). To determine whether a reduced AAK-2 signal in *pry-1* mutants is due to a lower abundance of protein, we examined GFP fluorescence in *aak-2p::aak-2::GFP* transgenic animals and found no change in fluorescence intensity in *pry-1(mu38)* mutants compared with that in the control (Figure S7D). Thus, PRY-1 is necessary for AAK-2 phosphorylation.

Three additional experiments support PRY-1 playing a role in AAK-2 activation: First, *pry-1* RNAi did not exacerbate the life span defect of *aak-2(ok524)* animals (Figure 7A; Table S2). Second, a constitutively active form of AMPKα2 (due to increased T172 phosphorylation), which causes a long-lived phenotype in worms (Mair et al., 2011), was unable to rescue the life span defect of *pry-1(mu38)* (Figure 7B; Table S2). And, three, *aak-2* is expressed in BWMs and neurons during adulthood in a pattern that resembles *pry-1* (Lee et al., 2008; Mair et al., 2011) (Figure S7E). Moreover, similar to *aak-2* mutants, *pry-1* mutant animals exhibited significantly reduced life span of dauers (55-70% reduction in mean life span in two different alleles compared to the control, $p < 0.01$) (Figure S7F; Table S2) (Narbonne and Roy, 2009). Taken together, these data support a model of PRY-1 promoting AAK-2 activation, likely through protein-protein interaction. The LKB1 homolog, PAR-4, required for AAK-2 activation (Lee et al., 2008) may also be involved in this process, since the life span defect of *par-4* mutant was not enhanced by *pry-1(RNAi)* (Figure S7G). The activated AAK-2 may, in turn, act in a cell non-autonomous manner to affect DAF-16 function in the intestine.

The model above suggests that PRY-1 and AAK-2 affect the expression of a common set of genes. Indeed, the transcriptome data sets of *pry-1* and *aak-2* mutants (Ranawade et al., 2018; Shin et al., 2011) showed a significant overlap (192 shared genes, 132 upregulated and 60 downregulated; RF: 1.2, hyp.geo $p < 0.006$) (Figure 7F; Table S7). Of these, 60 (45%) are mutually upregulated and 28 (47%) mutually downregulated in both mutants. The overlapping set of differentially expressed genes are linked to GO processes such as muscle structure development (*act-1, mel-26, unc-52, emb-9, unc-15,* and *unc-54*), muscle contraction (*unc-54*), aging (*daf-16, prmt-1, mpk-1, chc-1, cgh-1, dao-5,* and *glp-4*), lipid metabolic processes (*tat-4, ldp-1, sptl-3, pmt-1, lipin-1,* and *cgt-3*), and regulation of lipid localization (*daf-16, prmt-1, sams-1, tat-4, lea-1, vit-1, vit-3, vit-4,* and *vit-6*). Moreover, a significant number of genes are associated with stress response (27) and catabolic process (25) (Table S7).

To further investigate the interaction of *aak-2* with *pry-1*, tissue-specific knockdown experiments were performed. Both muscle and intestine-specific *aak-2* RNAi abolished life span extension in *unc-54p::pry-1* animals (Figures 7C and 7D; Table S2). Additionally, RNAi caused significantly fewer animals to show nuclear-localized DAF-16:GFP (Figures 7E and 7F). As with *aak-2*, RNAi knock-down of *par-4* in the muscle suppressed the life span extension of *unc-54p::pry-1* (Figure S7H), providing further evidence for PAR-4's

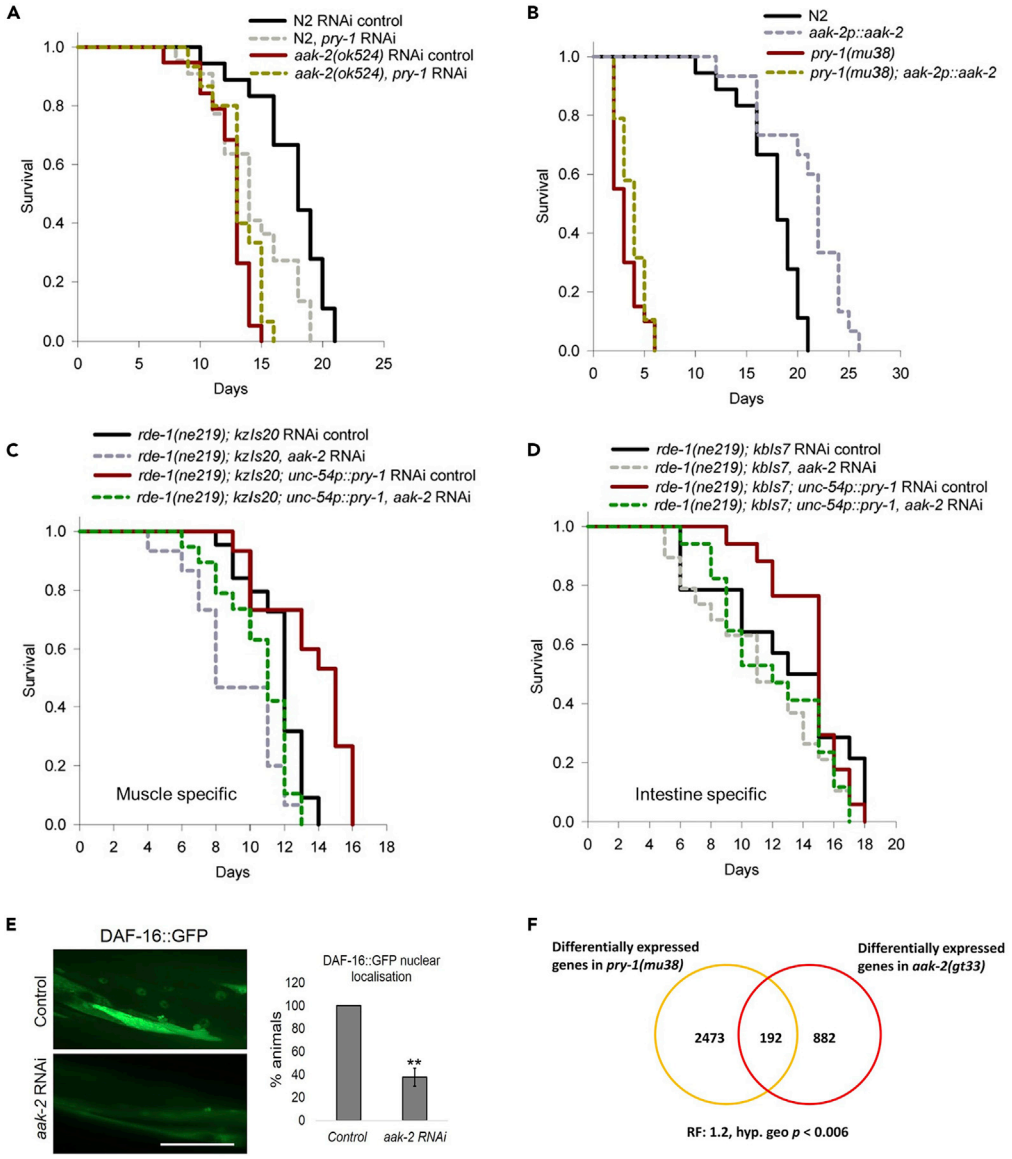

Figure 7. PRY-1 Interacts with AAK-2 to Regulate DAF-16 Localization and Life Span Extension

(A) *pry-1* RNAi knockdown in *aak-2(ok524)* animals.

(B) Constitutive activation of *aak-2* in *pry-1(mu38)* animals.

(C and D) *aak-2* RNAi knockdown in the muscle and intestine in *unc-54p::pry-1* animals.

(A–D) See Transparent Methods and Table S2 for life span data and statistical analyses.

(E) *aak-2* RNAi effect on DAF-16:GFP localization in *unc-54p::pry-1* animals. Scale bar is 50 μm.

Data represent the means of two replicates (15 animals each) and error bars the standard deviation. Significance was calculated using Student's t-test. **p < 0.01.

(F) Venn diagram showing an overlapping set of genes between *pry-1(mu38)* and *aak-2(gt33)* transcriptomes.

involvement in PRY-1 and AAK-2 interaction. Collectively, the results described in this section lead us to conclude that PRY-1 interacts with PAR-4 and AAK-2 in the muscle, thereby affecting DAF-16 localization in the intestine and, ultimately, the life span of animals.

DISCUSSION

Our results demonstrate the role of *C. elegans* Axin family member PRY-1 in life span maintenance, which involves AAK-2/AMPK-mediated DAF-16/FOXO signaling. We found that the *pry-1* mutant transcriptome

contains a significant number of aging-associated genes, including IIS and UPR^{ER} pathway components as well as those linked to lipid maintenance. Moreover, a significant number of DAF-16 direct targets are altered in *pry-1* mutants, and a majority of these are downregulated. Consistent with these findings, previous studies have shown that both DAF-16 and XBP-1-mediated UPR^{ER} signaling regulate stress response, lipid metabolism, and longevity (Imanikia et al., 2019; Lee et al., 2003; Lin et al., 2018; Murphy et al., 2003; Taylor and Dillin, 2013). As expected from misregulation of aging-related genes, a partial or complete loss of PRY-1 activity resulted in a shorter life span. The aging phenotype was associated with physiological changes such as slower rates of body bending and pharyngeal pumping, an increase in aging pigment (lipofuscin), and higher expression of UPR^{ER} and UPR^{MT} chaperones. Altogether, these data suggest that *pry-1* affects multiple conserved pathways involved in stress maintenance and aging.

The characterization of *pry-1* expression uncovered muscles as a major tissue for gene action. Other tissues showing a relatively lower abundance of *pry-1* include neurons, hypodermis, and intestine. Since the WNT ligands, *mom-2* and *cwn-2*, are localized in some of these tissues (Song et al., 2010) and both ligands affect life span (Lezzerini and Budovskaya, 2014), we investigated the possibility of *pry-1* acting in a WNT-dependent manner. The results of genetic interaction experiments suggest that *mom-2*-mediated signaling may affect *pry-1* function to maintain life span. However, such a mechanism may not involve the canonical WNT effector protein β-catenin. It is worth noting that WNT signaling has been shown to play roles in cellular senescence, aging, and age-related diseases (Brack et al., 2007; Gruber et al., 2016; Naito et al., 2010; Zhang et al., 2019). However, the regulation and function of Axin in the pathway is poorly understood.

The finding that *pry-1* is expressed in multiple tissues led us to investigate its tissue-specific function. The results of RNAi-mediated knockdowns and rescue experiments revealed that the gene is needed in the muscle and hypodermis to maintain life span. Interestingly, forced expression of *pry-1* in muscles, but not in hypodermis, allowed animals to live longer. Considering that Axin homologs are expressed in muscles (Smith et al., 2019; Uhlen et al., 2015) and mouse Axin (*mAxin1*) extended the life span of *C. elegans* when ectopically expressed in the muscle tissue, we propose that the beneficial role of Axin in the muscle is evolutionarily conserved.

pry-1's involvement in muscle health was further investigated using the transcriptome data, which uncovered a significant number of genes involved in muscle structure development and function. Almost all of these were downregulated. Another group of genes regulated by *pry-1* are associated with mitochondria and include those that function in the mitochondrial membrane, mitochondrial matrix, and mitochondrial ATP synthesis, suggesting that *pry-1* plays a major role in maintaining the health of this vital organelle. As expected, mutant animals showed increased fragmentation of mitochondria, which may contribute to muscle aging and a shorter life span (Gouspillou and Hepple, 2016; Hood et al., 2019; Mergoud Dit Lamarche et al., 2018). In contrast, muscle-specific overexpression of *pry-1* resulted in marked improvements in mitochondrial morphology and locomotion. The relationship between aging and muscle mitochondrial function is well described. For example, *daf-2* mutants that have a longer life span show preservation of mitochondrial morphology and delayed muscle aging (Mergoud Dit Lamarche et al., 2018; Wang et al., 2019). Additionally, *daf-16* is essential for the maintenance of muscle mitochondrial health (Wang et al., 2019). We found that both transcription and subcellular localization of DAF-16 is regulated by PRY-1. Moreover, genetic experiments revealed that the *pry-1*-mediated life span depends on *daf-16*. Interestingly, DAF-16 was nuclear localized in the intestine of *unc-54p::pry-1* worms. This localization appears to be important, since the intestine-specific knockdown of *daf-16* abolished the life span extension of transgenic animals.

We investigated the mechanism of PRY-1-mediated DAF-16 regulation and uncovered the role of AMPK homolog AAK-2 in this process. Specifically, PRY-1 is essential for the activation of AAK-2, which, in turn, promotes DAF-16 nuclear localization and life span extension of *unc-54p::pry-1* animals. Previous work has reported the involvement of AAK-2 in regulating DAF-16 function (Chen et al., 2013; Greer et al., 2007a). Hence, these data, along with genetic interactions, *aak-2::GFP* expression, and *pry-1* and *aak-2* transcriptome analysis, support the following model: PRY-1, PAR-4, and AAK-2 form a complex in the muscle, leading to AAK-2 phosphorylation. Activated AAK-2 initiates cell non-autonomous signaling to regulate DAF-16 activity in the intestine to maintain the life span. This model is consistent with the previously reported role of AAK-2 (Burkewitz et al., 2014).

One of the outcomes of *pry-1* interaction with *daf-16* could be to affect lipid metabolism, since lipids are implicated in aging (Papsdorf and Brunet, 2019) and both genes promote monounsaturated fatty acid

synthesis by transcriptionally regulating fatty acid desaturases such as *fat-7* (Murphy et al., 2003; Ranawade et al., 2018; Zhang et al., 2013a). Other possibilities are also likely because DAF-16 interacts with multiple factors to regulate life span (Lapierre and Hansen, 2012; Uno and Nishida, 2016). We should point out that AXL-1, another Axin homolog in *C. elegans*, was reported previously to be necessary for metformin-induced life span extension, although *axl-1* mutants have no aging-related phenotypes of their own (Chen et al., 2017). Thus, our work on PRY-1 provides the first evidence of an Axin family member regulating muscle health as well as life span.

Interactions between Axin and AMPK have been reported previously in mammalian systems. Specifically, the Axin-AMPK complex formation was enhanced in cultured cells when subjected to glucose deprivation, and Axin knockdown in the mouse liver impaired AMPK activation (Zhang et al., 2013b). AMPK is known to promote mitochondrial biogenesis and mitochondrial function in human umbilical vein cells and mice aorta (Marin et al., 2017). Moreover, AMPK phosphorylates all four human FOXO family members (Greer et al., 2007b). Similar to that with AMPK, AAK-2-mediated life span extension depends on mitochondrial network maintenance and DAF-16 regulation (Greer et al., 2007a; Uno and Nishida, 2016; Weir et al., 2017). Thus, it is plausible that Axin-AMPK-FOXO interact in a conserved manner to regulate disparate biological processes in eukaryotes. Studies in humans and other higher systems have established a connection between aging, muscle health, mitochondrial dysfunction, and diseases (Gouspillou and Hepple, 2016; Hood et al., 2019). Furthermore, Axin is essential for muscle maintenance, since myogenesis is abrogated in mutant animals (Huraskin et al., 2016) and *Axin2* upregulation is associated with increased muscle fibrosis in aging mice (Arthur and Cooley, 2012; Brack et al., 2007). Since muscle mass and function progressively decline with age, understanding the mechanism of Axin's function in this tissue promises to uncover potential interventions for aging-associated muscle deterioration.

Limitations of the Study

We have shown that *pry-1* is necessary to maintain muscle health and life span in *C. elegans*. However, it remains to be determined whether Axin homologs in other systems also regulate similar processes. Our conclusion that muscle-specific expression of *pry-1* extends life span is based on the analysis of transgenic animals that constitutively express the gene throughout developmental and post-developmental periods. In the future, it will be worthwhile to investigate *pry-1*'s role by activating its expression specifically during adulthood. The analysis of the *pry-1* role in muscles led us to investigate its interactions with *aak-2/AMPK* and *daf-16/FOXO*. While our data demonstrates that the muscle-specific expression of *pry-1* causes an increase in AAK-2 phosphorylation, whether PRY-1 physically interacts with AAK-2 is yet to be examined. Finally, we found that PRY-1-AAK-2-mediated signaling acts cell non-autonomously to promote nuclear localization of DAF-16 in the intestine, which is necessary for life span extension. However, the factors that facilitate communication between PRY-1 and DAF-16 remain to be identified.

Resource Availability

Lead Contact

Further information and requests for resources and reagents should be directed to and will be fulfilled by the Lead Contact, Bhagwati P Gupta (guptab@mcmaster.ca).

Materials Availability

All data generated or analyzed in this study are included in this published article and its supplemental information.

Data and Code Availability

The published article includes all data generated or analyzed during this study.

METHODS

All methods can be found in the accompanying Transparent Methods supplemental file.

SUPPLEMENTAL INFORMATION

Supplemental Information can be found online at https://doi.org/10.1016/j.isci.2020.101843.

ACKNOWLEDGMENTS

We thank Hannah Hosein, Sakshi Mehta and Lindyann Lessey for assistance with some of the experiments and Lesley MacNeil for providing feedback on the initial draft. Some of the strains were obtained from CGC, which is funded by the NIH Office of Research Infrastructure Programs (P40OD010440). The tissue-specific promoter plasmids were kindly provided by the Roy lab (McGill). This work was supported by NSERC Discovery grant to BG.

AUTHOR CONTRIBUTIONS

BG and AM designed the study. AM, AR, and WB performed the experiments. BG and AM analyzed the data and wrote the manuscript. All authors reviewed and edited the draft. BG supervised the project.

DECLARATION OF INTERESTS

The authors declare no competing interests.

Received: August 17, 2020
Revised: October 14, 2020
Accepted: November 17, 2020
Published: December 18, 2020

REFERENCES

Apfeld, J., O'Connor, G., McDonagh, T., DiStefano, P.S., and Curtis, R. (2004). The AMP-activated protein kinase AAK-2 links energy levels and insulin-like signals to lifespan in C. elegans. Genes Dev. *18*, 3004–3009.

Arthur, S.T., and Cooley, I.D. (2012). The effect of physiological stimuli on sarcopenia; impact of Notch and Wnt signaling on impaired aged skeletal muscle repair. Int. J. Biol. Sci. *8*, 731–760.

Bansal, A., Kwon, E.S., Conte, D., Jr., Liu, H., Gilchrist, M.J., MacNeil, L.T., and Tissenbaum, H.A. (2014). Transcriptional regulation of Caenorhabditis elegans FOXO/DAF-16 modulates lifespan. Longev Healthspan *3*, 5.

Benedetti, C., Haynes, C.M., Yang, Y., Harding, H.P., and Ron, D. (2006). Ubiquitin-like protein 5 positively regulates chaperone gene expression in the mitochondrial unfolded protein response. Genetics *174*, 229–239.

Brack, A.S., Conboy, M.J., Roy, S., Lee, M., Kuo, C.J., Keller, C., and Rando, T.A. (2007). Increased Wnt signaling during aging alters muscle stem cell fate and increases fibrosis. Science *317*, 807–810.

Burkewitz, K., Zhang, Y., and Mair, W.B. (2014). AMPK at the nexus of energetics and aging. Cell Metab. *20*, 10–25.

Chen, A.T., Guo, C., Itani, O.A., Budaitis, B.G., Williams, T.W., Hopkins, C.E., McEachin, R.C., Pande, M., Grant, A.R., Yoshina, S., et al. (2015). Longevity genes revealed by integrative analysis of isoform-specific daf-16/FoxO mutants of Caenorhabditis elegans. Genetics *201*, 613–629.

Chen, D., Li, P.W., Goldstein, B.A., Cai, W., Thomas, E.L., Chen, F., Hubbard, A.E., Melov, S., and Kapahi, P. (2013). Germline signaling mediates the synergistically prolonged longevity produced by double mutations in daf-2 and rsks-1 in C. elegans. Cell Rep. *5*, 1600–1610.

Chen, J., Ou, Y., Li, Y., Hu, S., Shao, L.W., and Liu, Y. (2017). Metformin extends C. elegans lifespan through lysosomal pathway. Elife *6*, e31268.

Davis, B.O., Jr., Anderson, G.L., and Dusenbery, D.B. (1982). Total luminescence spectroscopy of fluorescence changes during aging in Caenorhabditis elegans. Biochemistry *21*, 4089–4095.

de Lencastre, A., Pincus, Z., Zhou, K., Kato, M., Lee, S.S., and Slack, F.J. (2010). MicroRNAs both promote and antagonize longevity in C. elegans. Curr. Biol. *20*, 2159–2168.

Gouspillou, G., and Hepple, R.T. (2016). Editorial: mitochondria in skeletal muscle health, aging and diseases. Front. Physiol. *7*, 446.

Greer, E.L., Dowlatshahi, D., Banko, M.R., Villen, J., Hoang, K., Blanchard, D., Gygi, S.P., and Brunet, A. (2007a). An AMPK-FOXO pathway mediates longevity induced by a novel method of dietary restriction in C. elegans. Curr. Biol. *17*, 1646–1656.

Greer, E.L., Oskoui, P.R., Banko, M.R., Maniar, J.M., Gygi, M.P., Gygi, S.P., and Brunet, A. (2007b). The energy sensor AMP-activated protein kinase directly regulates the mammalian FOXO3 transcription factor. J. Biol. Chem. *282*, 30107–30119.

Gruber, J., Yee, Z., and Tolwinski, N.S. (2016). Developmental drift and the role of Wnt signaling in aging. Cancers (Basel) *8*, 73.

Hardie, D.G., and Lin, S.C. (2017). AMP-activated protein kinase - not just an energy sensor. F1000Res *6*, 1724.

Hardie, D.G., Ross, F.A., and Hawley, S.A. (2012). AMPK: a nutrient and energy sensor that maintains energy homeostasis. Nat. Rev. Mol. Cell Biol. *13*, 251–262.

Hood, D.A., Memme, J.M., Oliveira, A.N., and Triolo, M. (2019). Maintenance of skeletal muscle mitochondria in health, exercise, and aging. Annu. Rev. Physiol. *81*, 19–41.

Huang, C., Xiong, C., and Kornfeld, K. (2004). Measurements of age-related changes of physiological processes that predict lifespan of Caenorhabditis elegans. Proc. Natl. Acad. Sci. U S A *101*, 8084–8089.

Huraskin, D., Eiber, N., Reichel, M., Zidek, L.M., Kravic, B., Bernkopf, D., von Maltzahn, J., Behrens, J., and Hashemolhosseini, S. (2016). Wnt/beta-catenin signaling via Axin2 is required for myogenesis and, together with YAP/Taz and Tead1, active in IIa/IIx muscle fibers. Development *143*, 3128–3142.

Imanikia, S., Sheng, M., Castro, C., Griffin, J.L., and Taylor, R.C. (2019). XBP-1 remodels lipid metabolism to extend longevity. Cell Rep. *28*, 581–589 e584.

Kenyon, C. (2011). The first long-lived mutants: discovery of the insulin/IGF-1 pathway for ageing. Philos. Trans. R. Soc. Lond. B Biol. Sci. *366*, 9–16.

Kenyon, C., Chang, J., Gensch, E., Rudner, A., and Tabtiang, R. (1993). A C. elegans mutant that lives twice as long as wild type. Nature *366*, 461–464.

Kenyon, C.J. (2010). The genetics of ageing. Nature *464*, 504–512.

Korswagen, H.C., Coudreuse, D.Y., Betist, M.C., van de Water, S., Zivkovic, D., and Clevers, H.C. (2002). The Axin-like protein PRY-1 is a negative regulator of a canonical Wnt pathway in *C. elegans*. Genes Dev. *16*, 1291–1302.

Kwon, E.S., Narasimhan, S.D., Yen, K., and Tissenbaum, H.A. (2010). A new DAF-16 isoform regulates longevity. Nature *466*, 498–502.

Lapierre, L.R., and Hansen, M. (2012). Lessons from C. elegans: signaling pathways for longevity. Trends Endocrinol. Metab. *23*, 637–644.

Lee, H., Cho, J.S., Lambacher, N., Lee, J., Lee, S.J., Lee, T.H., Gartner, A., and Koo, H.S. (2008). The Caenorhabditis elegans AMP-activated protein kinase AAK-2 is phosphorylated by LKB1 and is required for resistance to oxidative stress and for normal motility and foraging behavior. J. Biol. Chem. *283*, 14988–14993.

Lee, S.S., Kennedy, S., Tolonen, A.C., and Ruvkun, G. (2003). DAF-16 target genes that control C. elegans life-span and metabolism. Science *300*, 644–647.

Lezzerini, M., and Budovskaya, Y. (2014). A dual role of the Wnt signaling pathway during aging in Caenorhabditis elegans. Aging Cell *13*, 8–18.

Li, Y.H., and Zhang, G.G. (2016). Towards understanding the lifespan extension by reduced insulin signaling: bioinformatics analysis of DAF-16/FOXO direct targets in Caenorhabditis elegans. Oncotarget *7*, 19185–19192.

Libina, N., Berman, J.R., and Kenyon, C. (2003). Tissue-specific activities of C. elegans DAF-16 in the regulation of lifespan. Cell *115*, 489–502.

Lin, X.X., Sen, I., Janssens, G.E., Zhou, X., Fonslow, B.R., Edgar, D., Stroustrup, N., Swoboda, P., Yates, J.R., 3rd, Ruvkun, G., et al. (2018). DAF-16/FOXO and HLH-30/TFEB function as combinatorial transcription factors to promote stress resistance and longevity. Nat. Commun. *9*, 4400.

Lopez-Otin, C., Blasco, M.A., Partridge, L., Serrano, M., and Kroemer, G. (2013). The hallmarks of aging. Cell *153*, 1194–1217.

Madeo, F., Zimmermann, A., Maiuri, M.C., and Kroemer, G. (2015). Essential role for autophagy in life span extension. J. Clin. Invest. *125*, 85–93.

Mair, W., Morantte, I., Rodrigues, A.P., Manning, G., Montminy, M., Shaw, R.J., and Dillin, A. (2011). Lifespan extension induced by AMPK and calcineurin is mediated by CRTC-1 and CREB. Nature *470*, 404–408.

Mallick, A., and Gupta, B.P. (2020). Vitellogenin-2 acts downstream of PRY-1/Axin to regulate lipids and lifespan in C. elegans. Micropubl Biol. *21*, 2020.

Mallick, A., Ranawade, A., and Gupta, B.P. (2019a). Role of PRY-1/Axin in heterochronic miRNA-mediated seam cell development. BMC Dev. Biol. *19*, 17.

Mallick, A., Taylor, S.K.B., Ranawade, A., and Gupta, B.P. (2019b). Axin family of scaffolding proteins in development: lessons from C. elegans. J. Dev. Biol. *7*, 20.

Marin, T.L., Gongol, B., Zhang, F., Martin, M., Johnson, D.A., Xiao, H., Wang, Y., Subramaniam, S., Chien, S., and Shyy, J.Y. (2017). AMPK promotes mitochondrial biogenesis and function by phosphorylating the epigenetic factors DNMT1, RBBP7, and HAT1. Sci. Signal. *10*, eaaf7478.

Melendez, A., Talloczy, Z., Seaman, M., Eskelinen, E.L., Hall, D.H., and Levine, B. (2003). Autophagy genes are essential for dauer development and life-span extension in C. elegans. Science *301*, 1387–1391.

Mergoud Dit Lamarche, A., Molin, L., Pierson, L., Mariol, M.C., Bessereau, J.L., Gieseler, K., and Solari, F. (2018). UNC-120/SRF independently controls muscle aging and lifespan in Caenorhabditis elegans. Aging Cell *17*, e12713.

Mihaylova, M.M., and Shaw, R.J. (2011). The AMPK signalling pathway coordinates cell growth, autophagy and metabolism. Nat. Cell Biol. *13*, 1016–1023.

Murphy, C.T., McCarroll, S.A., Bargmann, C.I., Fraser, A., Kamath, R.S., Ahringer, J., Li, H., and Kenyon, C. (2003). Genes that act downstream of DAF-16 to influence the lifespan of Caenorhabditis elegans. Nature *424*, 277–283.

Naito, A.T., Shiojima, I., and Komuro, I. (2010). Wnt signaling and aging-related heart disorders. Circ. Res. *107*, 1295–1303.

Narbonne, P., and Roy, R. (2009). Caenorhabditis elegans dauers need LKB1/AMPK to ration lipid reserves and ensure long-term survival. Nature *457*, 210–214.

Ogg, S., Paradis, S., Gottlieb, S., Patterson, G.I., Lee, L., Tissenbaum, H.A., and Ruvkun, G. (1997). The Fork head transcription factor DAF-16 transduces insulin-like metabolic and longevity signals in C. elegans. Nature *389*, 994–999.

Papsdorf, K., and Brunet, A. (2019). Linking lipid metabolism to chromatin regulation in aging. Trends Cell Biol. *29*, 97–116.

Ranawade, A., Mallick, A., and Gupta, B.P. (2018). PRY-1/Axin signaling regulates lipid metabolism in Caenorhabditis elegans. PLoS One *13*, e0206540.

Regmi, S.G., Rolland, S.G., and Conradt, B. (2014). Age-dependent changes in mitochondrial morphology and volume are not predictors of lifespan. Aging (Albany NY) *6*, 118–130.

Ron, D., and Walter, P. (2007). Signal integration in the endoplasmic reticulum unfolded protein response. Nat. Rev. Mol. Cell Biol. *8*, 519–529.

Seetharaman, A., Cumbo, P., Bojanala, N., and Gupta, B.P. (2010). Conserved mechanism of Wnt signaling function in the specification of vulval precursor fates in C. elegans and C. briggsae. Dev. Biol. *346*, 128–139.

Shin, H., Lee, H., Fejes, A.P., Baillie, D.L., Koo, H.S., and Jones, S.J. (2011). Gene expression profiling of oxidative stress response of C. elegans aging defective AMPK mutants using massively parallel transcriptome sequencing. BMC Res. Notes *4*, 34.

Smith, C.M., Hayamizu, T.F., Finger, J.H., Bello, S.M., McCright, I.J., Xu, J., Baldarelli, R.M., Beal, J.S., Campbell, J., Corbani, L.E., et al. (2019). The mouse gene expression database (GXD): 2019 update. Nucleic Acids Res. *47*, D774–D779.

Song, S., Zhang, B., Sun, H., Li, X., Xiang, Y., Liu, Z., Huang, X., and Ding, M. (2010). A Wnt-Frz/Ror-Dsh pathway regulates neurite outgrowth in Caenorhabditis elegans. PLoS Genet. *6*, e1001056.

Stenesen, D., Suh, J.M., Seo, J., Yu, K., Lee, K.S., Kim, J.S., Min, K.J., and Graff, J.M. (2013). Adenosine nucleotide biosynthesis and AMPK regulate adult life span and mediate the longevity benefit of caloric restriction in flies. Cell Metab. *17*, 101–112.

Taylor, R.C., and Dillin, A. (2013). XBP-1 is a cell-nonautonomous regulator of stress resistance and longevity. Cell *153*, 1435–1447.

Tran, H.C., and Van Aken, O. (2020). Mitochondrial unfolded protein-related responses across kingdoms: similar problems, different regulators. Mitochondrion *53*, 166–177.

Twig, G., and Shirihai, O.S. (2011). The interplay between mitochondrial dynamics and mitophagy. Antioxid. Redox Signal. *14*, 1939–1951.

Uhlen, M., Fagerberg, L., Hallstrom, B.M., Lindskog, C., Oksvold, P., Mardinoglu, A., Sivertsson, A., Kampf, C., Sjostedt, E., Asplund, A., et al. (2015). Proteomics. Tissue-based map of the human proteome. Science *347*, 1260419.

Uno, M., and Nishida, E. (2016). Lifespan-regulating genes in C. elegans. NPJ Aging Mech. Dis. *2*, 16010.

Wang, H., Webster, P., Chen, L., and Fisher, A.L. (2019). Cell-autonomous and non-autonomous roles of daf-16 in muscle function and mitochondrial capacity in aging C. elegans. Aging (Albany NY) *11*, 2295–2311.

Weir, H.J., Yao, P., Huynh, F.K., Escoubas, C.C., Goncalves, R.L., Burkewitz, K., Laboy, R., Hirschey, M.D., and Mair, W.B. (2017). Dietary restriction and AMPK increase lifespan via mitochondrial network and peroxisome remodeling. Cell Metab. *26*, 884–896 e885.

Xu, Y., He, Z., Song, M., Zhou, Y., and Shen, Y. (2019). A microRNA switch controls dietary restriction-induced longevity through Wnt signaling. EMBO Rep. *20*, e46888.

Zhang, P., Judy, M., Lee, S.J., and Kenyon, C. (2013a). Direct and indirect gene regulation by a life-extending FOXO protein in C. elegans: roles for GATA factors and lipid gene regulators. Cell Metab. *17*, 85–100.

Zhang, Q., Wu, X., Chen, P., Liu, L., Xin, N., Tian, Y., and Dillin, A. (2018). The mitochondrial unfolded protein response is mediated cell-non-autonomously by retromer-dependent Wnt signaling. Cell *174*, 870–883 e817.

Zhang, Y., Jeffrey, J., Dong, F., Zhang, J., Kao, W.W., Liu, C.Y., and Yuan, Y. (2019). Repressed Wnt signaling accelerates the aging process in mouse eyes. J. Ophthalmol. *2019*, 7604396.

Zhang, Y.L., Guo, H., Zhang, C.S., Lin, S.Y., Yin, Z., Peng, Y., Luo, H., Shi, Y., Lian, G., Zhang, C., et al. (2013b). AMP as a low-energy charge signal autonomously initiates assembly of AXIN-AMPK-LKB1 complex for AMPK activation. Cell Metab. *18*, 546–555.

Zhou, B., Kreuzer, J., Kumsta, C., Wu, L., Kamer, K.J., Cedillo, L., Zhang, Y., Li, S., Kacergis, M.C., Webster, C.M., et al. (2019). Mitochondrial permeability uncouples elevated autophagy and lifespan extension. Cell *177*, 299–314 e216.

iScience, Volume *23*

Supplemental Information

Axin-Mediated Regulation of Lifespan and Muscle Health in *C. elegans* Requires AMPK-FOXO Signaling

Avijit Mallick, Ayush Ranawade, Wouter van den Berg, and Bhagwati P. Gupta

SUPPLEMENTAL INFORMATION

Supplementary Figures

Figure S1: *pry-1* expression in older adults, effect of *pry-1* overexpression on lifespan, and phenotype of *C. briggsae pry-1* mutant, related to Figures 1, and 4.
(A) qPCR analysis showing *pry-1* transcript levels at day-1, 4 and 8 of adulthood. Data represent the means of two replicates and error bars represent the SEM. Significance was calculated using Bio-Rad software (t-test). *$p < 0.05$.
(B) Lifespan phenotype of *hs::pry-1* transgenic animals.
(C) Lifespan phenotype of *Cbr-pry-1(sy5353)* mutant.
(B-C) See Transparent methods and Table S2 for lifespan data and statistical analyses.

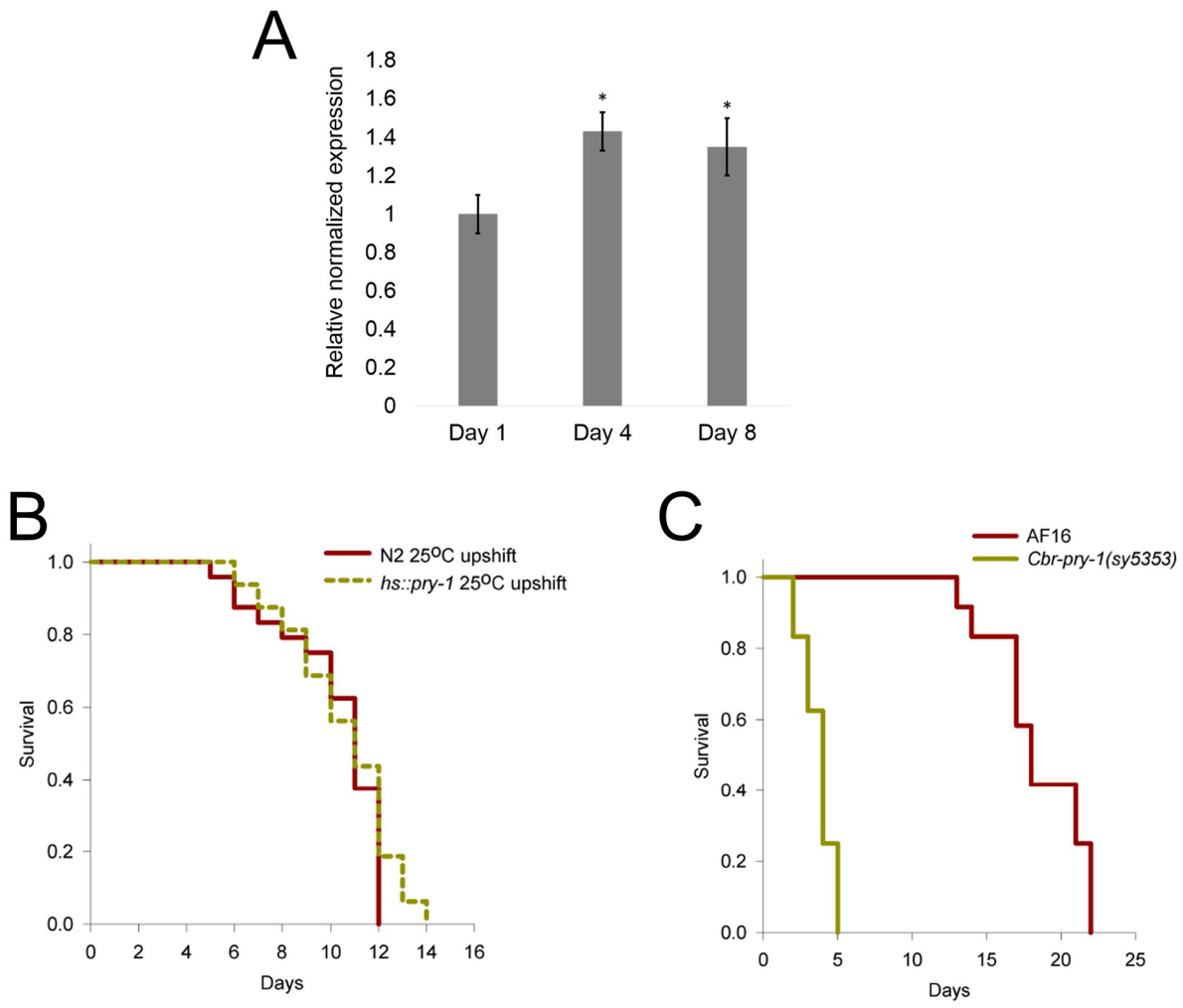

Figure S2: Analysis of pharyngeal pumping and body bending in *pry-1(mu38)* animals, related to Figure 2.

(A and B) Pharyngeal pumping and body bending rates in the *pry-1* mutants.

(C and D) Rescue of *pry-1(mu38)* defects by expression of *pry-1* transgene using a *hs::pry-1* construct.

(A-D) Data represent the means of at least two replicates (n ≥ 30 animals) and error bars the standard deviation. Significance was calculated using Student's t-test *$p < 0.05$, **$p < 0.01$.

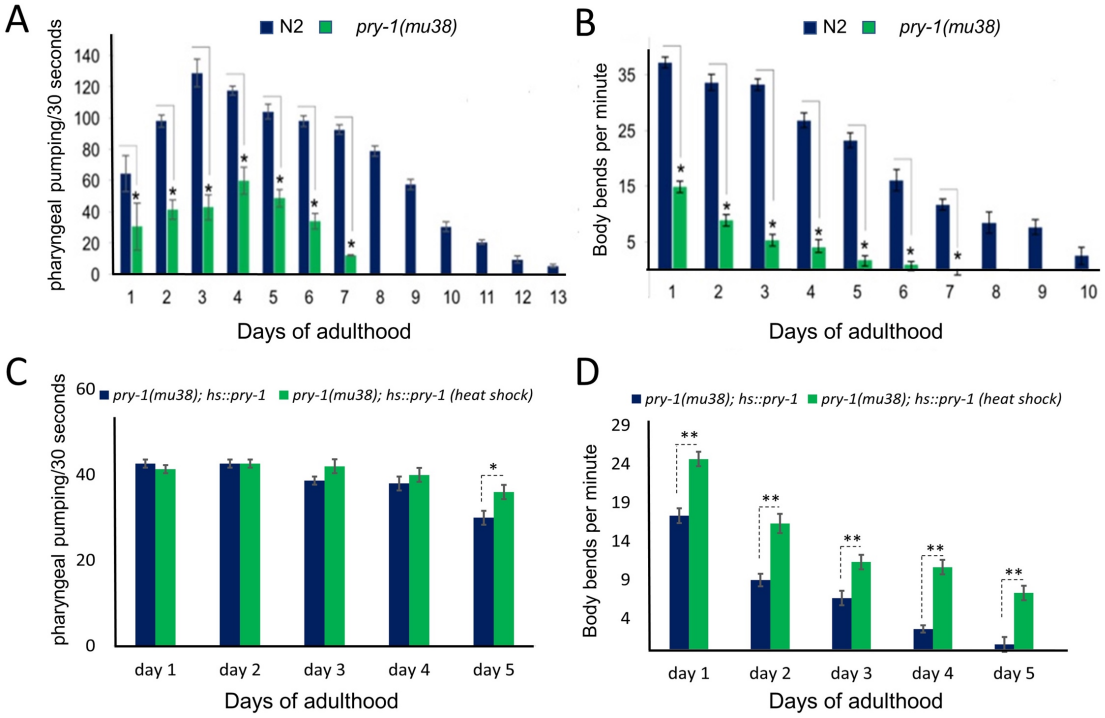

Figure S3: Expression pattern of *pry-1* in *C. elegans*, related to Figure 4.
(A) Expression pattern of *pry-1* in *pry-1p::pry-1::GFP* transgenic animals during larval and adult stages.
(B) Magnified image showing GFP fluorescence in body wall muscles. Nuclei are indicated by arrows.
(C) Arrows point to intestinal nuclei showing GFP fluorescence.

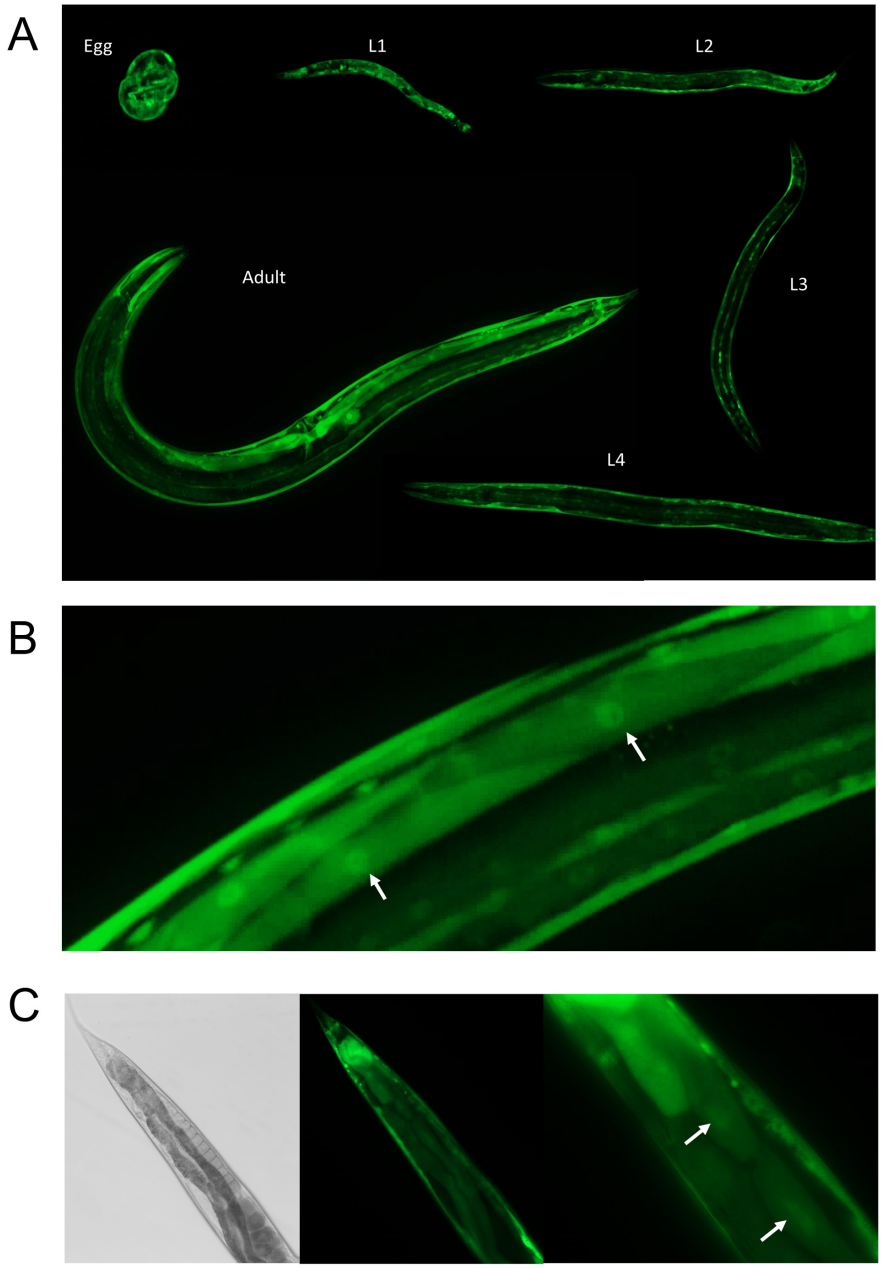

Figure S4: Expression pattern of *pry-1* in *C. briggsae* and the impact of tissue-specific knockdowns of *C. elegans pry-1* on lifespan, related to Figure 4.
(A) Representative images of *C. briggsae pry-1p::GFP* transgenic animals showing GFP fluorescence in muscles of an L4 larva and an adult.
(B) Lifespan phenotype of animals following *pry-1* RNAi knockdown in neurons.
(C) Lifespan phenotype of animals following *pry-1* RNAi knockdown in intestine, hypodermis and germline.
(B-C) See Transparent methods and Table S2 for lifespan data and statistical analyses.

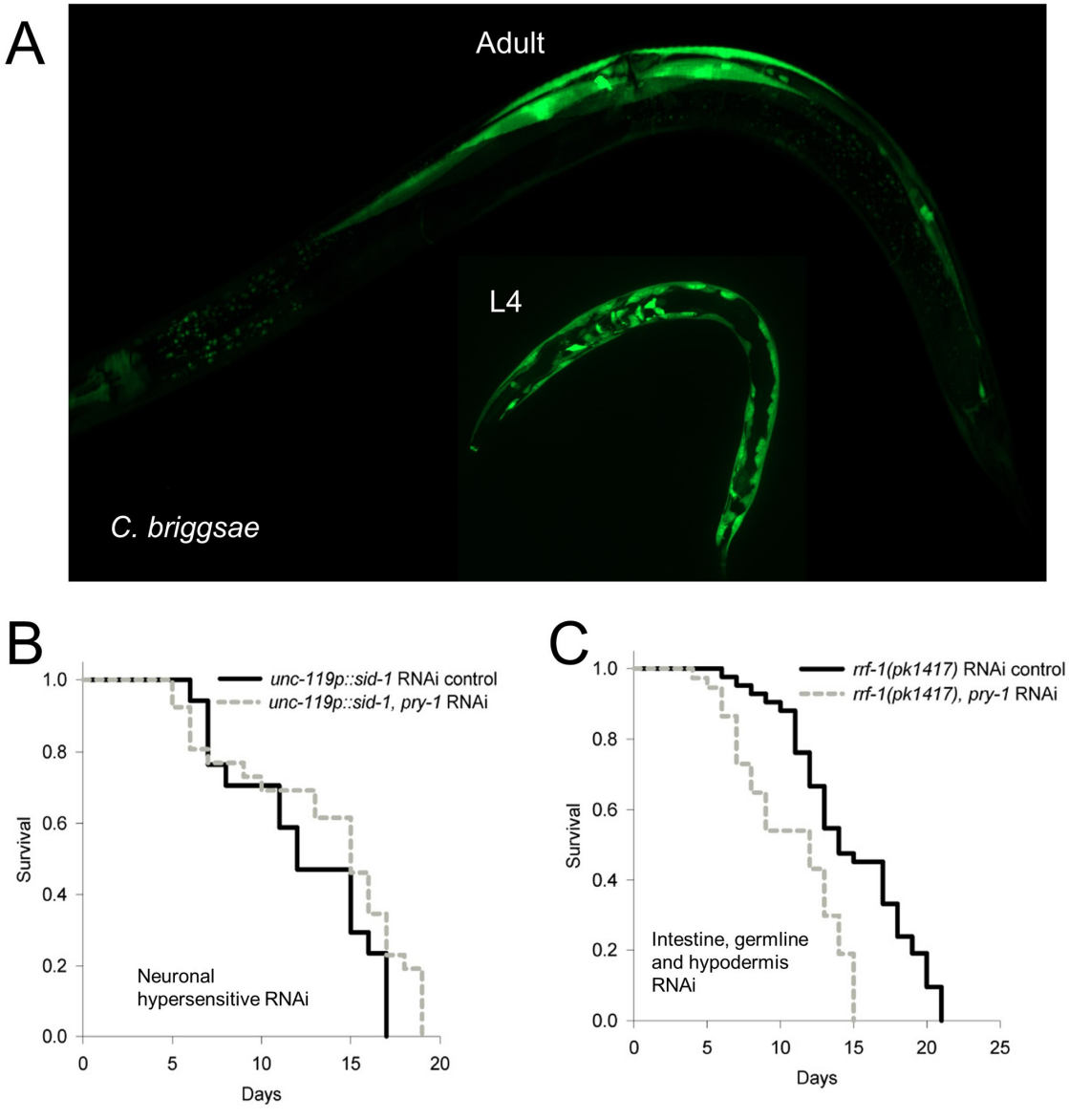

Figure S5: Rescue analysis of *pry-1(mu38)* lifespan defect and the effect of muscle-specific expression of mouse Axin1 in *C. elegans*, related to Figure 5.

(A and B) Lifespan rescue experiments by tissue-specific expression of *pry-1* in hypodermis (A) and muscle.

(C) Lifespan phenotype of animals expressing *mAxin1* in the muscle.

(A-C) See Transparent methods and Table S2 for lifespan data and statistical analyses.

(D and E) Rates of body bending and pharyngeal pumping in *unc-54p::pry-1* animals.

(F) Thrashing rate of *unc-54p::pry-1* between day 8 and 11.

(D-F) Data represent the means of at least two replicates (30 animals each) and error bars the standard deviation. Significance was calculated using Student's t-test *$p < 0.05$, **$p < 0.01$.

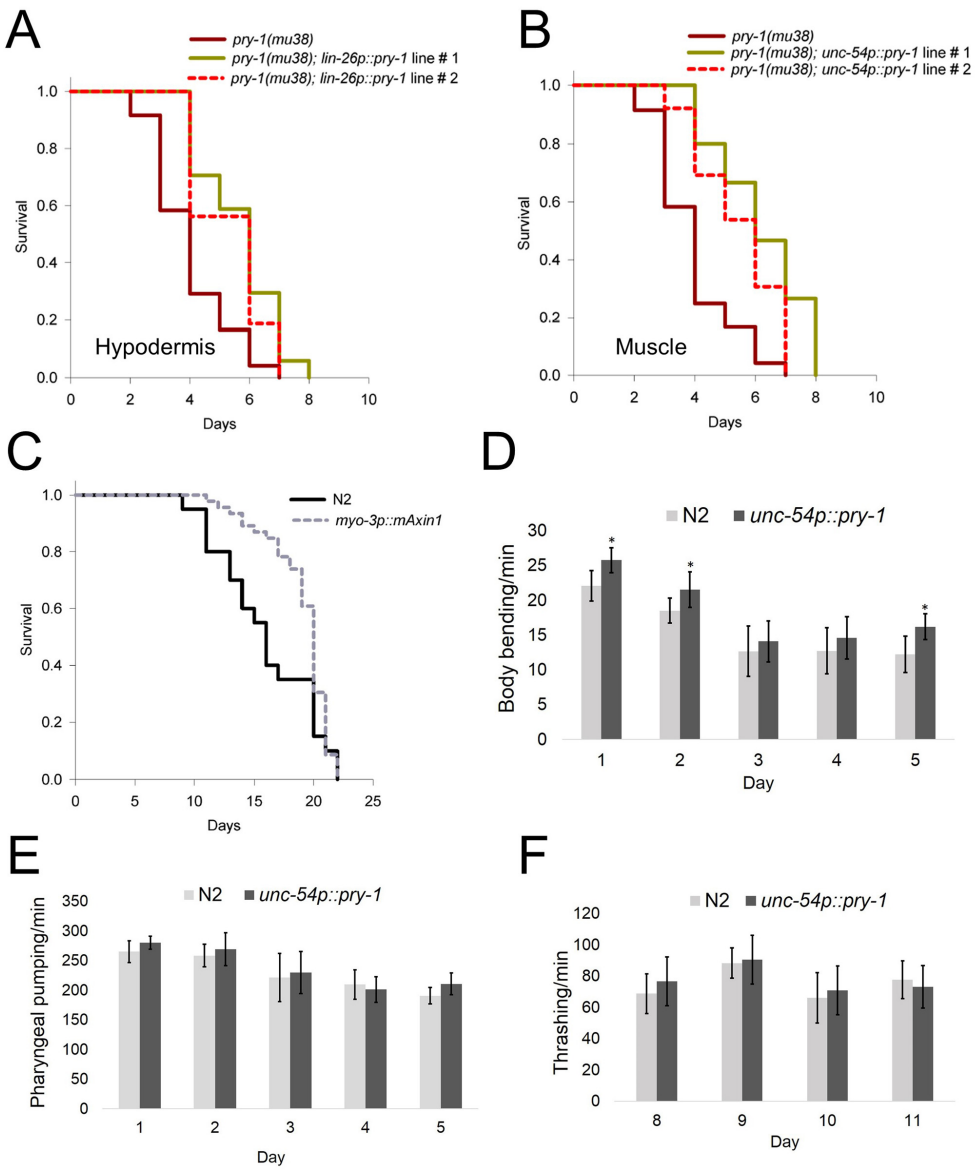

Figure S6: Expression of *daf-16* isoforms, GATA factors *elt-2* and *elt-4*, and *sod-3*. Genetic interactions of *pry-1* with *daf-2* and *daf-16*, related to Figure 6.

(A and B) Transcript levels of *daf-16a, daf-16d/f/h/i/k* and *daf-16* overall in day-1 *pry-1* mutants (A) and *unc-54p::pry-1* animals (B).

(C) Transcript levels of *elt-2* and *elt-4* in day-1 *unc-54p::pry-1* animals.

(A-C) Data represent the means of two replicates and error bars the SEM. Significance was calculated using Bio-Rad software (t-test). **p* < 0.05, ***p* < 0.01.

(D) Lifespan phenotype of *daf-2* mutants following *pry-1* RNAi.

(E) Lifespan phenotype of *pry-1(mu38); hs::pry-1* animals following *daf-16* RNAi.

(D and E) See Transparent methods and Table S2 for lifespan data and statistical analyses.

(F) *sod-3* transcript analysis in *unc-54p::pry-1* animals. Data represents the mean of two replicates and error bar the SEM. Significance was calculated using Bio-Rad software (t-test). **p* < 0.05, ***p* < 0.01.

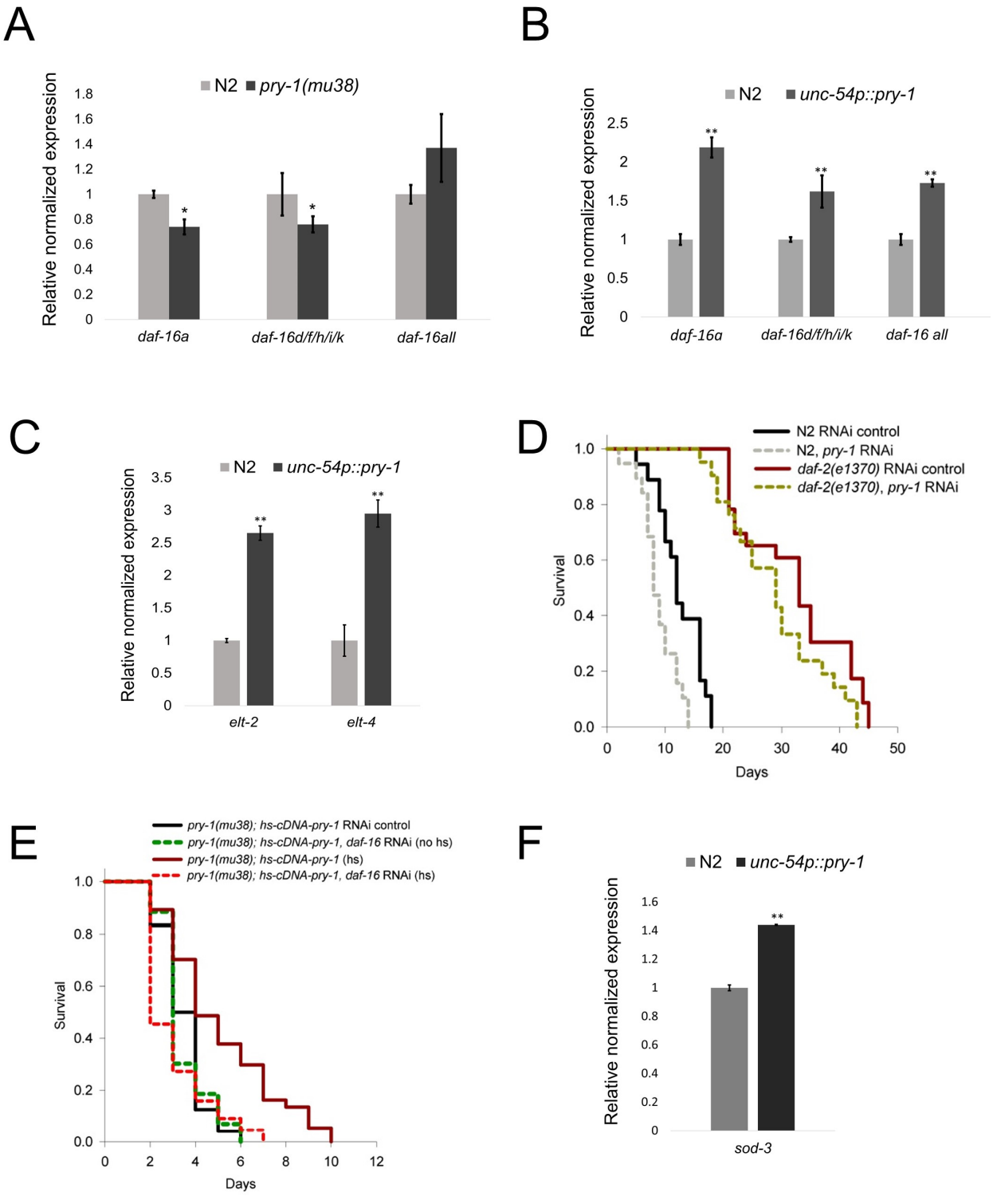
A
N2
pry-1(mu38)
Relative normalized expression
daf-16a
daf-16d/f/h/i/k
daf-16all
B
N2
unc-54p::pry-1
Relative normalized expression
daf-16a
daf-16d/f/h/i/k
daf-16 all
C
N2
unc-54p::pry-1
Relative normalized expression
elt-2
elt-4
D
N2 RNAi control
N2, pry-1 RNAi
daf-2(e1370) RNAi control
daf-2(e1370), pry-1 RNAi
Survival
Days
E
pry-1(mu38); hs-cDNA-pry-1 RNAi control
pry-1(mu38); hs-cDNA-pry-1, daf-16 RNAi (no hs)
pry-1(mu38); hs-cDNA-pry-1 (hs)
pry-1(mu38); hs-cDNA-pry-1, daf-16 RNAi (hs)
Survival
Days
F
N2
unc-54p::pry-1
Relative normalized expression
sod-3

Figure S7: Analyses of lipid levels and expression of genes involved in lipid synthesis in *unc-54p::pry-1* animals and genetic interactions of *aak-2* and *par-4* with *pry-1*, related to Figure 7.

(A) Oil red O staining of total lipid droplets in control and *unc-54p::pry-1* day-1 adults. Scale bar is 0.1mm.

(B) Quantification of lipid levels in animals shown in panel A. Data represent the means of at least two replicates ($n \geq 20$ animals each) and error bars the standard deviation. Significance was calculated using Student's t-test, $^{**}p < 0.01$.

(C) qPCR analysis of fatty acid desaturases (*fat-5, fat-6*, and *fat-7*) and SREBP homolog (*sbp-1*) in wild-type (N2) and *unc-54p::pry-1* day-1 adults. Data represent the means of two replicates and error bar the SEM. Significance was calculated using Bio-Rad software (t-test). $^{*}p < 0.05$, $^{**}p < 0.01$.

(D) Representative images of AAK-2::GFP in control and *pry-1(mu38)* animals. Scale bar is 0.2mm. Data represent the means of at least two replicates ($n \geq 20$ animals each) and error bars the standard deviation. Significance was calculated using Student's t-test, $^{**}p < 0.01$.

(E) Representative images of AAK-2::GFP animals. GFP fluorescence is visible in the muscle (arrowhead). Scale bar is 0.1mm.

(F) Dauer survivability phenotype of *pry-1(mu38), pry-1(gk3682),* and *aak-2(ok524)* animals.

(G) Lifespan analysis of *par-4(it57)* animals following control and *pry-1* RNAi knockdowns.

(H) Muscle-specific knockdown of *par-4* in control and *unc-54p::pry-1* animals.

(F-H) See Transparent methods and Table S2 for lifespan data and statistical analyses.

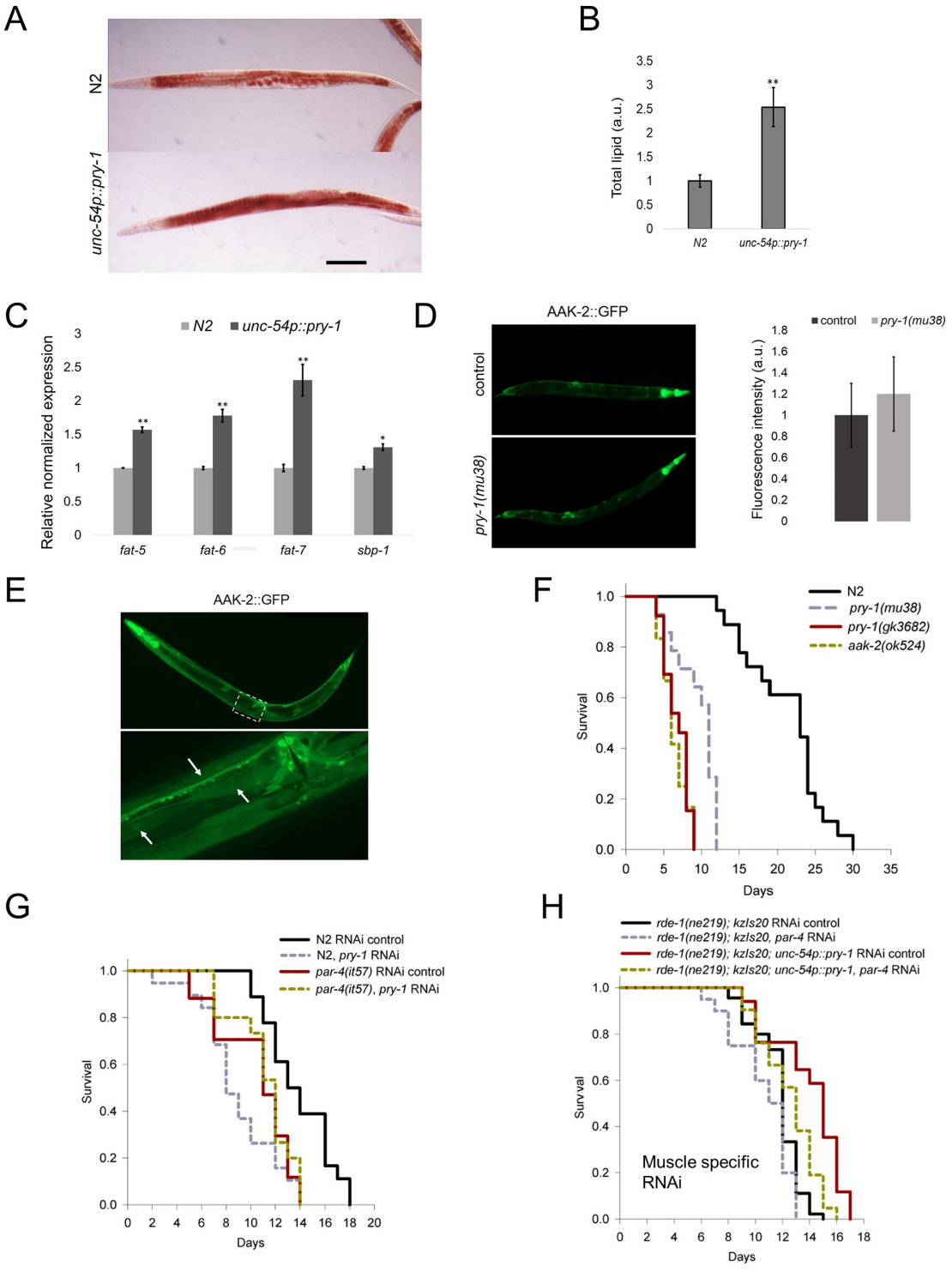
A
N2
unc-54p::pry-1
B
Total lipid (a.u.)
N2
unc-54p::pry-1
C
N2
unc-54p::pry-1
Relative normalized expression
fat-5
fat-6
fat-7
sbp-1
D
AAK-2::GFP
control
pry-1(mu38)
control
pry-1(mu38)
Fluorescence intensity (a.u.)
E
AAK-2::GFP
F
N2
pry-1(mu38)
pry-1(gk3682)
aak-2(ok524)
Survival
Days
G
N2 RNAi control
N2, pry-1 RNAi
par-4(it57) RNAi control
par-4(it57), pry-1 RNAi
Survival
Days
H
rde-1(ne219); kzIs20 RNAi control
rde-1(ne219); kzIs20, par-4 RNAi
rde-1(ne219); kzIs20; unc-54p::pry-1 RNAi control
rde-1(ne219); kzIs20; unc-54p::pry-1, par-4 RNAi
Survival
Muscle specific RNAi
Days

TRANSPARENT METHODS

LEAD CONTACT AND MATERIALS AVAILABILITY

Further information and requests for resources and reagents should be directed to and will be fulfilled by the Lead Contact, Bhagwati Gupta (guptab@mcmaster.ca).

EXPERIMENTAL MODEL AND SUBJECT DETAILS

Worm cultures

C. elegans strains (see Table S8) were maintained on nematode growth medium (NGM) agar-containing plates seeded with OP50 *E. coli* bacteria (Brenner, 1974). Cultures were kept at 20^0C unless otherwise stated.

Strain construction

DY230 strain was created by injecting 100 ng/µl of pGLC37 plasmid into the *pry-1(mu38)* animals. To generate transgenic animals (DY664-668), pGLC153(*unc-54p::pry-1*) or pGLC154(*lin-26p::pry-1*) was injected in N2 animals at 30 ng/µL along with 30 ng/µL of pPD136.64(*myo-3p::YFP*) marker. Two independent lines were established in each case. pGLC153 was also co-injected with 30 ng/µL pPD136.64 in the strains NR350 and VP303 to generate muscle (DY682) and intestine-specific (DY690) RNAi lines. DY679 was generated by injecting 30ng/µL pDC10(*pry-1p::pry-1::GFP*) and co-injection marker 10ng/µL *dat-1p::mCherry* in N2. pDC10 was injected in *C. briggsae* AF16 animals to generate the strain DY160.

METHOD DETAILS

Reagents and resources used in this study are listed in Table S8.

Plasmid construction

pGLC37 was constructed by subcloning full-length *C37A5.9/pry-1* cDNA (1.7kb) downstream of *hsp-16-41* promoter in the vector pPD49.83.

unc-54p::pry-1 plasmid (pGLC153), containing PRY-1 cDNA downstream of muscle-specific promoter *unc-54*, was constructed as follows. Three different fragments, 4.1kbp of *unc-54* promoter, 1.7kbp of *pry-1*-cDNA from pGLC37, and 646bp of *unc-54* 3' UTR from genomic DNA were amplified using primers (Table S8). The purified fragments were cloned into the destination vector using the Multisite Gateway Pro (Thermo Fisher Scientific) protocol.

lin-26p::pry-1 plasmid (pGLC154), containing PRY-1 cDNA downstream of the hypodermis-specific promoter *lin-26*, was constructed as follows. Three different fragments, 4.1kbp of *lin-26*-promoter, 1.7kbp of *pry-1*-cDNA from pGLC37, and 646bp of

unc-54 3' UTR from genomic DNA were amplified using primers (Table S8). The purified fragments were cloned into the destination vector using the Multisite Gateway Pro (Thermofisher) protocol.

pDC10 was kindly provided by Hendrick Korswagen (Korswagen et al., 2002). The plasmid contains a genomic DNA fragment including the complete *C37A5.9/pry-1*-coding sequence and 3.6 kb of upstream sequence inserted in-frame into the *GFP* reporter containing vector pPD95.81.

pry-1 RNAi plasmid (pGLC142) was constructed by inserting a genomic fragment of 2.3kb into the L4440 vector using restriction enzymes *Hind*III and *Xma*I. The fragment was obtained by PCR using the primers GL1343 and GL1344.

RNA extraction and qPCR

Total RNA was extracted from one large plate of worms using the Trizol-based extraction procedure (SIGMA). RNA was DNAse treated according to a protocol (QIAGEN). 1 µg of RNA was used to synthesize cDNA using a SensiFAST cDNA synthesis kit (BIOLINE). SYBR Green (BIORAD) quantitative RT-PCR was performed using the BIORAD CFX-Real Time system and following the BIORAD-CFX Software manual. Data from three biological repeats were analyzed using the comparative 2ΔΔCt method and significance assessed by one-way ANOVA.

RNAi

RNAi-mediated gene silencing was performed using the protocol previously published by our laboratory (Seetharaman et al., 2010). For adult specific RNAi, synchronized worms were cultivated on plates containing OP50 bacteria until the young adult stage and then transferred to RNAi plates. Either L4440 empty vector or GFP RNAi bacteria was used as a control (Kamath et al., 2001). RNAi knockdown of *bar-1* in *pry-1(mu38); hs::pry-1* strain had no effect on the lifespan but did suppress the multivulva phenotype of animals.

RNA-seq data analysis

RNA-seq data for *pry-1(mu38)* animals were published (Ranawade et al., 2018) and deposited in NCBI with accession number GEO GSE94412. GO analysis was carried out with default setting using GoAmigo (http://amigo.geneontology.org). A GO-term containing at least three genes with a *p*-value adjusted for multiple comparisons and < 0.05 (Benjamini-Hochberg method) was counted significant (Carbon et al., 2009). Tissue enrichment analysis was performed using WormBase online TEA tool that employs a tissue ontology (Angeles-Albores et al., 2016).

Lifespan analysis

Lifespan analysis was carried out following an established protocol (Amrit et al., 2014). Each strain was repeated at least twice. A minimum of 50 animals were used per condition, and worms were scored for viability every second day, from day 1 of adulthood (treating the pre-fertile day preceding adulthood as t = 0). *daf-2(e1370)* and *par-4(it57)* animals were grown at 25^0C after reaching adulthood. Young adult worms were transferred to fresh plates every other day and the numbers of dead worms were recorded as events scored. Animals that were lost or burrowed in the medium, exhibiting protruding vulva (intestine protrudes from the vulva), or undergoing bagging (larvae hatching inside the worm body) were censored. SigmaPlot software was used for statistical analysis, and *p* values were calculated using the log-rank (Kaplan-Meier) method.

Dauer longevity assay

Dauers were generated using a starvation protocol. Synchronized gravid adults were plated and allowed to lay eggs for 8 hours following which adults were removed. The plate was then shifted to 27^0C and after 3 days 10 Dauer larvae were randomly picked into a 20 µl drop of double-distilled water suspended under a Petri dish cover. A wet tissue was placed on the bottom of the plate and was sealed with Parafilm. Dauer longevity was monitored daily at 25^oC, and survival was scored as moving response upon exposure to a focused beam of 425-440 nm light as previously described (Narbonne and Roy, 2006). SigmaPlot software was used for statistical analysis, and *p* values were calculated using the log-rank (Kaplan-Meier) method.

Pharyngeal pumping and locomotion

Pharyngeal pumping assay was performed on NGM plates containing a thin bacterial lawn. Worms were bleach synchronized and allowed to grow in the presence of food to late L4 stage. 10 worms were transferred to assay plates, and the number of contractions in the terminal bulb of the pharynx of each animal was counted every 24 hours for 30 sec using a Nikon 80i inverted microscope. Four independent experiments were performed on each day.

The locomotion rate of worms on different days of adulthood was examined using a protocol from the Sternberg lab. Briefly, worms were bleach synchronized and allowed to grow till late L4 stage. Five worms were placed onto separate plates and tested daily for locomotion until death. For testing, a worm was picked onto an NGM plate containing a uniform layer of bacteria and stimulated by contact with the tail. The number of body movements was counted from the trail left on the plate.

Oil Red O staining

Oil Red O (Sigma-Aldrich) staining was performed following the standard protocol (Ranawade et al 2018). Worms were washed with 1x PBS buffer (pH 7.4), and re-

suspended in 60 µl of 1x PBS, 120 µl of 2x MRWB buffer and 60 µl of 4% paraformaldehyde. The worms were then freeze-thawed three times and washed twice with 1x PBS. They were then incubated at room temperature in 60% isopropyl alcohol for 10 minutes for dehydration and stained with freshly prepared Oil Red O solution for at least 48 hours on a shaker. Animals were imaged with a Q-imaging software and Micropublisher 3.3 RTV color camera outfitted with DIC optics on a Nikon 80i microscope. NIH ImageJ software was used to quantify Oil Red O intensities (Soukas et al., 2009). 15 to 30 worms were randomly selected from each category in at least two separate batches.

Fluorescence microscopy

Photomicrographs of GFP-tagged animals were acquired using Axiovision Zeiss microscope (Mallick et al., 2019). Nematodes were mounted on glass slides containing 2% agarose and 0.02M NaN_3 and quickly observed under the microscope (within 10 min.) to minimize stress. The microscopy analysis was independently replicated at least twice.

Western blotting

For native extracts, nematodes were synchronized by bleaching and allowed to grow on OP50 bacteria until day-1 of adulthood. Worms were then washed three times with M9 buffer, pelleted, and mixed with 1mL of native lysis buffer (as described in Gidalevitz et al., 2009). Samples were frozen in -80°C prior to use. Nematodes were thawed on ice and mechanically disrupted using a Precellys (Bertin Instruments) programmed for 8x10s pulses, with 30s between each pulse. Samples were then centrifuged for 5 minutes (13000 g) at 4^0C and supernatant containing total proteins was transferred to fresh tubes.

SDS-PAGE was carried out followed by electrophoretic transfer to nitrocellulose membrane at 100 V for 1 hour at 4°C. Immunoblots were performed according to primary antibody manufacturers' protocols. AAK-2 phosphorylation was probed with rabbit p-AMPKα (T172) antibody (CST). GAPDH was probed as housekeeping gene with 1:1000 mouse GAPDH (Invitrogen). Secondary antibodies, goat-anti-rabbit HRP-linked IgG (CST) and goat-anti-mouse IgG (Invitrogen), were diluted 1:1000 and 1:1500, respectively in 4% milk dissolved in TBST. Signal was detected using Amersham™ ECL™ Western Blotting Detection Reagent (GE Healthcare). The results are representative of two independent experiments.

Quantification and statistical analyses

For lifespan and stress resistance assays, statistics analyses were performed using SigmaPlot software 11. Survival curves were estimated using the Kaplan- Meier test and differences among groups were assessed using the log-rank test. Survival data are expressed relative to the control group. Bio-Rad CFX software was used for qPCR statistical analyses using t-test or one-way ANOVA.

Statistical analyses other than those for muscle mitochondrial morphology were performed using Microsoft Office Excel 365. The mitochondrial data was analyzed using GraphPad prism and p values were calculated using Fisher's exact test. Figure 5 shows values based on normal (tubular) and defective (intermediate and fragmented, combined) mitochondrial phenotypes. Significance was also determined for individual defective categories. The p values are: <0.0001, 0.7583, 0.0429, and 0.048 when comparing tubular with intermediate and <0.0001, 0.5128, 0.0110, and 0.0986 when comparing tubular with fragmented. The genotypes in both cases are: *pry-1(mu38),* whole-animal *pry-1*(RNAi), muscle-specific *pry-1* RNAi, and *unc-54p::pry-1,* respectively. We used the chi square test as well and obtained the following *p* values: <0.0001 for *pry-1(mu38)*, 0.5697 for whole-animal *pry-1*(RNAi), 0.0194 for muscle-specific *pry-1* RNAi, and 0.066 for *unc-54p::pry-1.*

In all cases, differences were considered statistically significant at $p < 0.05$, thereby indicating a probability of error lower than 5%. For hypergeometric probability testing, an online program (http://nemates.org/MA/progs/overlap_stats.html) was used to test statistical significance of the overlap between two gene sets.

Supplemental References

Amrit, F.R.G., Ratnappan, R., Keith, S.A., Ghazi, A., 2014. The *C. elegans* lifespan assay toolkit. Methods 68, 465–475. https://doi.org/10.1016/j.ymeth.2014.04.002

Angeles-Albores, D., Raymond, R.Y., Chan, J., Sternberg, P.W., 2016. Tissue enrichment analysis for *C. elegans* genomics. BMC Bioinformatics 17, 1–10. https://doi.org/10.1186/s12859-016-1229-9

Brenner, S., 1974. The genetics of *Caenorhabditis elegans*. Genetics 77, 71–94. https://doi.org/10.1002/cbic.200300625

Carbon, S., Ireland, A., Mungall, C.J., Shu, S., Marshall, B., Lewis, S., Lomax, J., Mungall, C., Hitz, B., Balakrishnan, R., Dolan, M., Wood, V., Hong, E., Gaudet, P., 2009. AmiGO: Online access to ontology and annotation data. Bioinformatics 25, 288–289. https://doi.org/10.1093/bioinformatics/btn615

Gidalevitz, T., Krupinski, T., Garcia, S., Morimoto, R.I., 2009. Destabilizing protein polymorphisms in the genetic background direct phenotypic expression of mutant SOD1 toxicity. PLoS Genet. 5. https://doi.org/10.1371/journal.pgen.1000399

Kamath, R.S., Martinez-Campos, M., Zipperlen, P., Fraser, A.G., Ahringer, J., 2001. Effectiveness of specific RNA-mediated interference through ingested double-stranded RNA in *Caenorhabditis elegans*. Genome Biol. 2, 1–10. https://doi.org/10.1186/gb-2000-2-1-research0002

Korswagen, H., Coudreuse, D., Betist, M., Water, S., Zivkovic, D., Clevers, H., 2002. The Axin-like protein PRY-1 is a negative regulator of a canonical Wnt pathway in

C. elegans. Genes Dev. 16, 1291–1302.

Mallick, A., Ranawade, A., Gupta, B.P., 2019. Role of PRY-1/Axin in heterochronic miRNA-mediated seam cell development. BMC Dev. Biol. 19, 1–12. https://doi.org/10.1186/s12861-019-0197-5

Narbonne, P., Roy, R., 2006. Inhibition of germline proliferation during *C. elegans* dauer development requires PTEN, LKB1 and AMPK signalling. Development 133, 611–619. https://doi.org/10.1242/dev.02232

Ranawade, A., Mallick, A., Gupta, B.P., 2018. PRY-1/Axin signaling regulates lipid metabolism in *Caenorhabditis elegans*. PLoS One 13, e0206540. https://doi.org/10.1371/journal.pone.0206540

Seetharaman, A., Cumbo, P., Bojanala, N., Gupta, B.P., 2010. Conserved mechanism of Wnt signaling function in the specification of vulval precursor fates in *C. elegans* and *C. briggsae*. Dev. Biol. 346, 128–139. https://doi.org/10.1016/j.ydbio.2010.07.003

Soukas, A.A., Kane, E.A., Carr, C.E., Melo, J.A., Ruvkun, G., 2009. Rictor/TORC2 regulates fat metabolism, feeding, growth, and life span in *Caenorhabditis elegans.* Genes Dev. 496–511. https://doi.org/10.1101/gad.1775409.2004